地下宇宙
2020.1.6.

星観測からの宇宙化学進化

青木和光
国立天文台

星観測からの宇宙化学進化

- 化学進化モデルへの制限
  Age-metallicity relation
  Metallicity distribution function
  Chemical abundance ratios
  →星の年齢、化学組成
- 動力学進化モデルへの制限
  →銀河系内の星の軌道運動

● 星の化学組成の測定
● 星の化学組成からの化学進化への制限
  例:リチウム

星の年齢の測定（制限）

Comparison with isochrone in HR diagram

- Nearby stars (Main-sequence turn-off stars/ subgiants)

- Red giants
  Accurate distance ←Gaia
  Evolutionary status　←seismology

Estimate from mass of red giants

- Empirical relation between stellar mass and seismology parameters (scaling relation)

Measurements of nearby stars: Age estimates

Nordstrom et al. (2004)

lines: Isochrones for 0-15 Gyr

Absolute magnitude

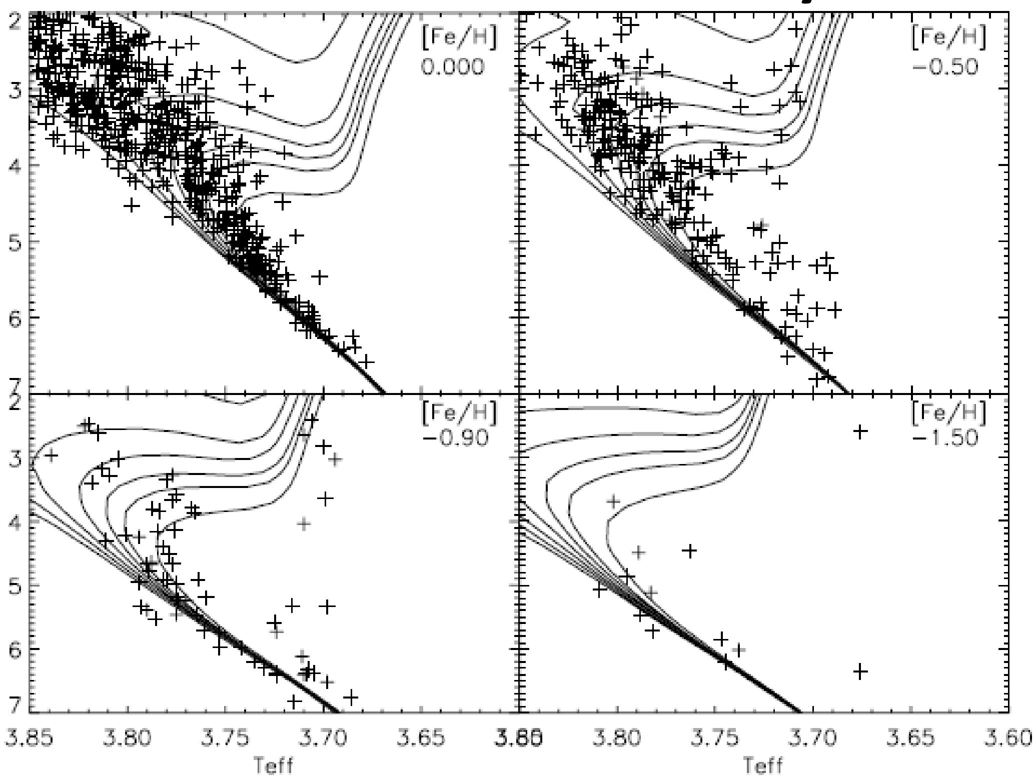

Effective temperature

Metallicity

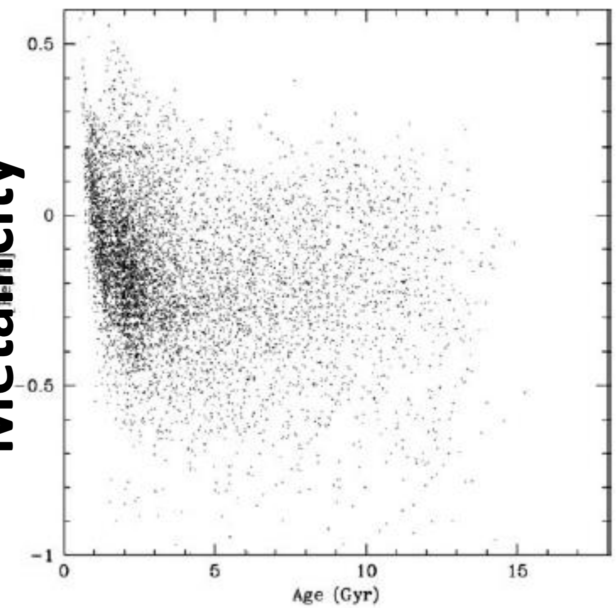

Age

Age estimate for red giants and clump stars by seismology with Kepler

Mosser et al. (2012) → Age metallicity relation *(Takeda et al. 2016)*

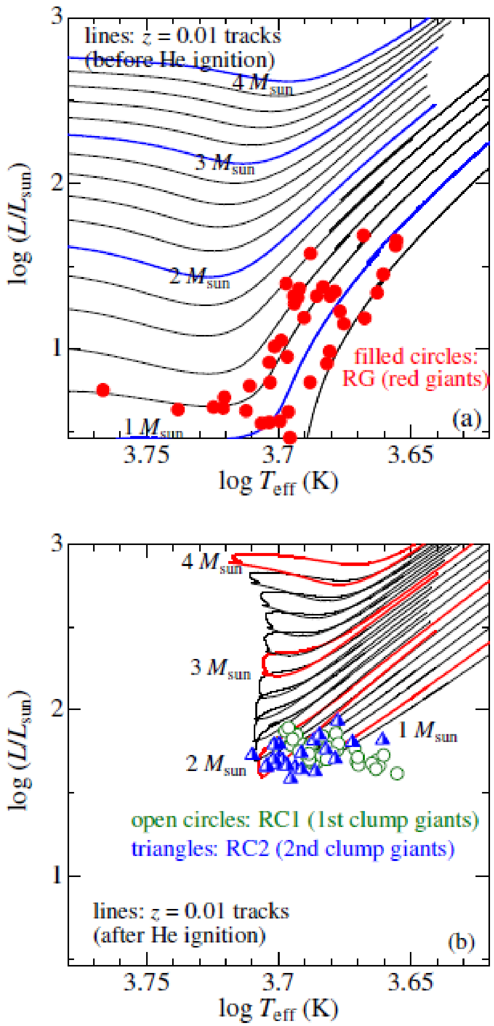

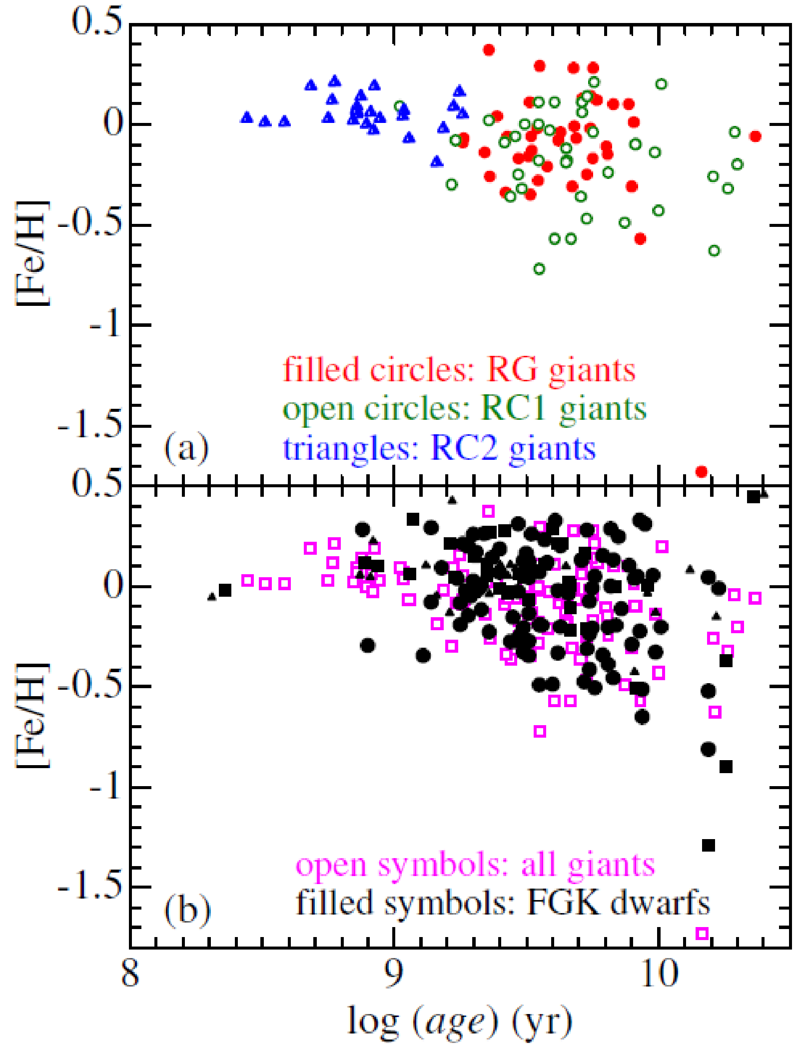

星の化学組成の測定

- 化学組成測定の実際
  - スペクトル線の測定
  - 恒星大気モデル
- 化学組成測定の不定性、信頼性
- 恒星の表面組成と元素の特性
- 太陽組成
- 同位体組成

Definition

- **Chemical abundance**： abundance ratio with respect to H

  $\log \varepsilon(X) = \log(X/H)+12$

  ex. $Fe/H=10^{-4.5}$ → $\log \varepsilon(Fe)=7.5$

  $[X/Y] = \log(X/Y)-\log(X/Y)_{sun}$

  例：$[Fe/H]=-2.0$ → 1/100 of the solar Fe/H ratio

- **Metallicity**： total abundance of heavy elements (elements heavier than boron)

  important for stellar structure and evolution

  sometimes presented as mass ratio

  ex. Solar metallicity = 0.02 (2%) or slightly lower

  usually represented by [Fe/H]

Solar abundance table (example)

Asplund et al. (2009)

Table 1 Element abundances in the present-day solar photosphere. Also given are the corresponding values for CI carbonaceous chondrites (Lodders, Palme & Gail 2009). Indirect photospheric estimates have been used for the noble gases (Section 3.9)

Z	Element	Photosphere	Meteorites	Z	Element	Photosphere	Meteorites
1	H	12.00	8.22 ± 0.04	44	Ru	1.75 ± 0.08	1.76 ± 0.03
2	He	[10.93 ± 0.01]	1.29	45	Rh	0.91 ± 0.10	1.06 ± 0.04
3	Li	1.05 ± 0.10	3.26 ± 0.05	46	Pd	1.57 ± 0.10	1.65 ± 0.02
4	Be	1.38 ± 0.09	1.30 ± 0.03	47	Ag	0.94 ± 0.10	1.20 ± 0.02
5	B	2.70 ± 0.20	2.79 ± 0.04	48	Cd		1.71 ± 0.03
6	C	8.43 ± 0.05	7.39 ± 0.04	49	In	0.80 ± 0.20	0.76 ± 0.03
7	N	7.83 ± 0.05	6.26 ± 0.06	50	Sn	2.04 ± 0.10	2.07 ± 0.06
8	O	8.69 ± 0.05	8.40 ± 0.04	51	Sb		1.01 ± 0.06
9	F	4.56 ± 0.30	4.42 ± 0.06	52	Te		2.18 ± 0.03
10	Ne	[7.93 ± 0.10]	−1.12	53	I		1.55 ± 0.08
11	Na	6.24 ± 0.04	6.27 ± 0.02	54	Xe	[2.24 ± 0.06]	−1.95
12	Mg	7.60 ± 0.04	7.53 ± 0.01	55	Cs		1.08 ± 0.02
13	Al	6.45 ± 0.03	6.43 ± 0.01	56	Ba	2.18 ± 0.09	2.18 ± 0.03
14	Si	7.51 ± 0.03	7.51 ± 0.01	57	La	1.10 ± 0.04	1.17 ± 0.02
15	P	5.41 ± 0.03	5.43 ± 0.04	58	Ce	1.58 ± 0.04	1.58 ± 0.02
16	S	7.12 ± 0.03	7.15 ± 0.02	59	Pr	0.72 ± 0.04	0.76 ± 0.03

Absorption in stellar spectra
→ “equivalent widths” (等価幅）

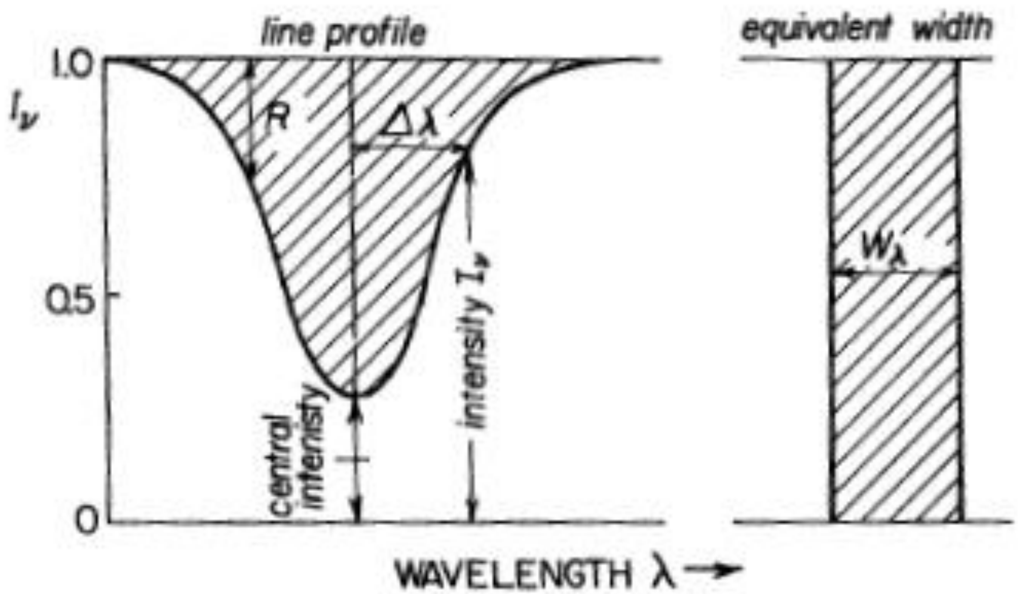

Fig. 3.4. Definition of equivalent width.

Pagel 1997

Equivalent width dose not change by broadening of stellar rotation and of instrument’s resolution.

Measurements of equivalent widths

- Gaussian fitting
- Fitting of Vogt profile
- Direct integration

Measurement errors

- S/N, continuum estimate
- Fitting error
- contamination

Abundances and line strengths

「成長曲線」

curve of growth

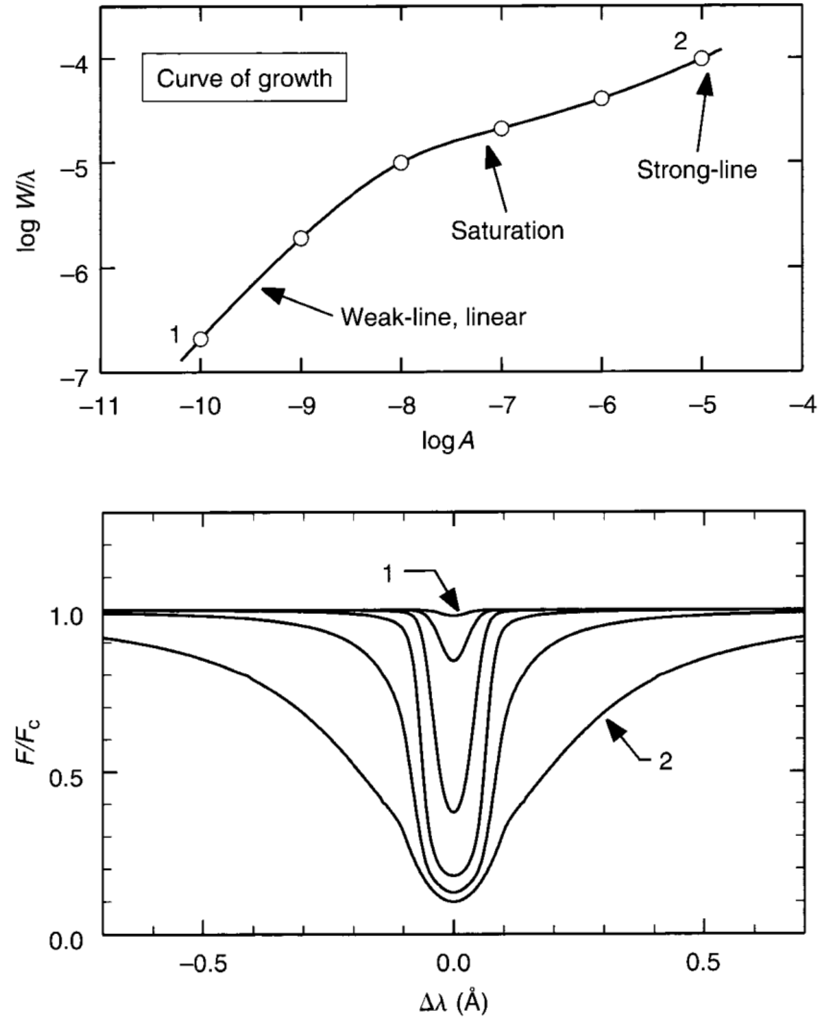

Fig. 13.11. Both the equivalent width (top) and the profile (bottom) change with chemical abundance of the absorbing species. The dots on the curve of growth correspond to the profiles below. Models have $S_0 = 0.87$ and $\log g = 4.0\,\mathrm{cm/s^2}$.

Absorption line strengths and abundance measurements

- **Measurements from weak lines**

○ line strength is in proportion to abundance

→not severely model dependent

× difficulty in line detection, sensitive to S/N of data

× sensitive to contamination of other lines

- **Measurements from strong lines**

○ easy to detect lines, measurement of line can be accurate (though Gaussian fitting is not applicable.)

× insensitive to abundances

→low accuracy in abundance determination

dependent on treatment of line broadening

× line formation in upper photosphere, for which modeling is difficult in general

Stellar atmosphere and its modeling

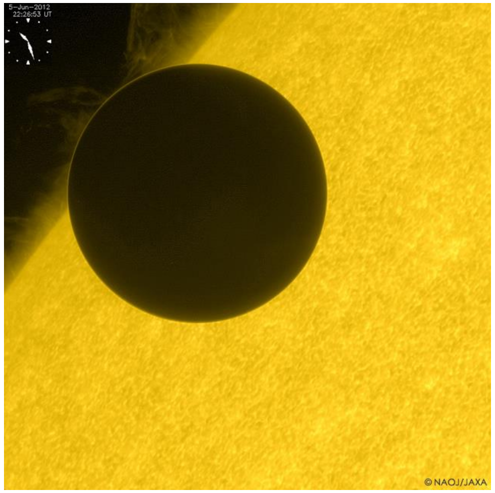

Solar atmosphere with Venus (Hinode)

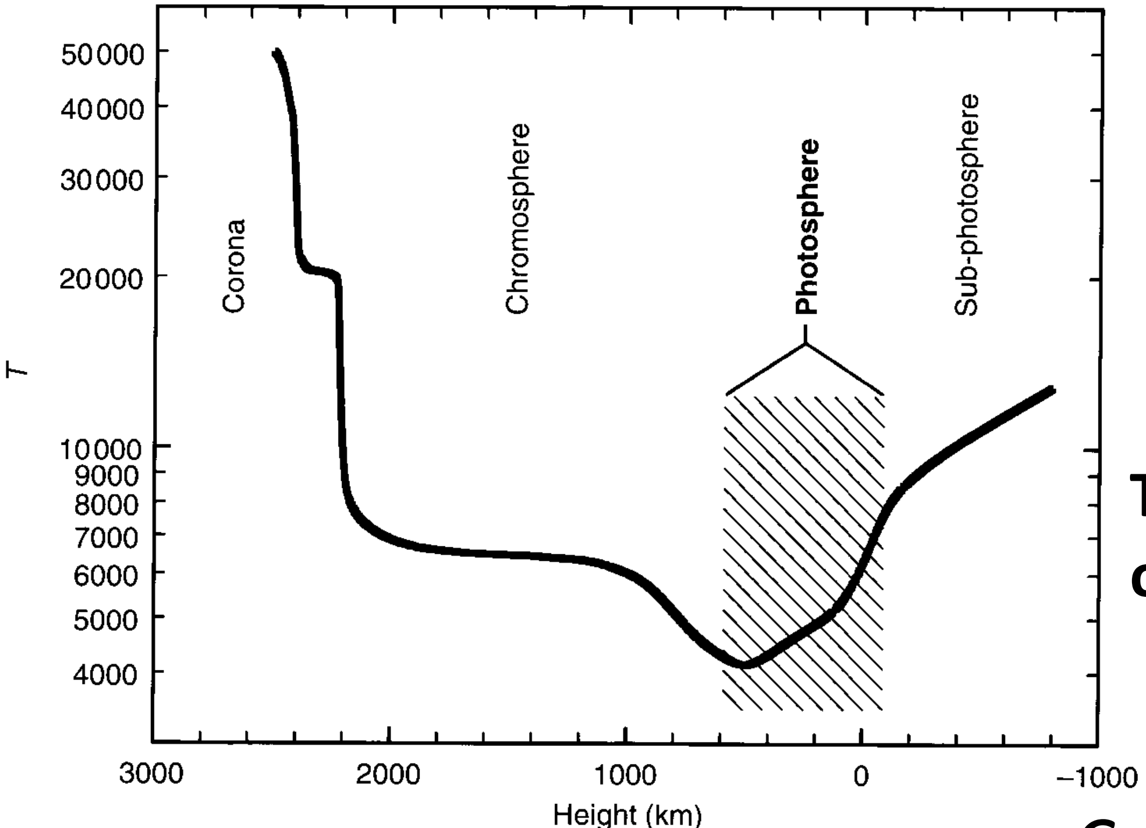

Temperature structure of the solar atmosphere

Gray 2005

Stellar atmosphere and spectra

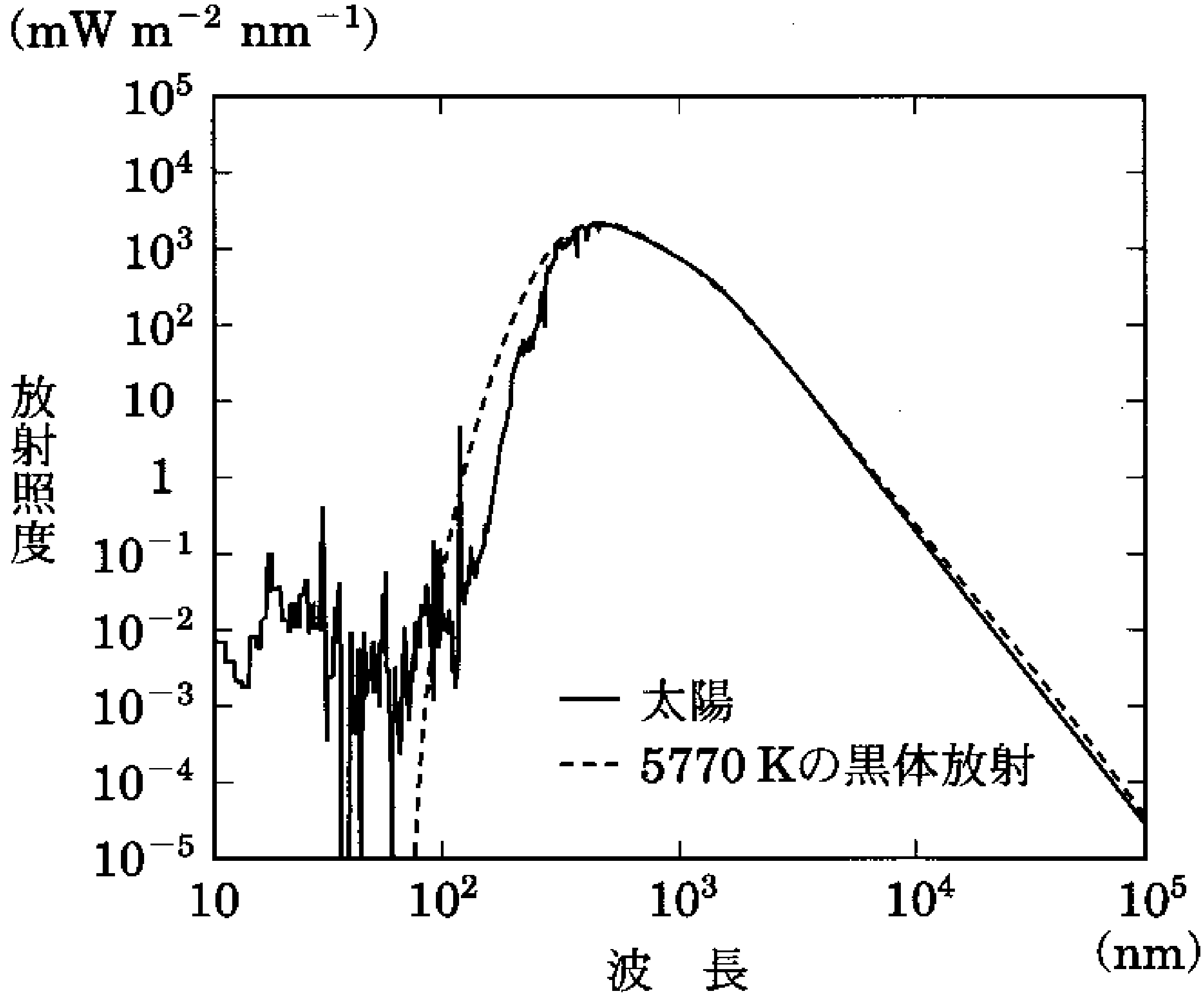

Modeling the solar photosphere

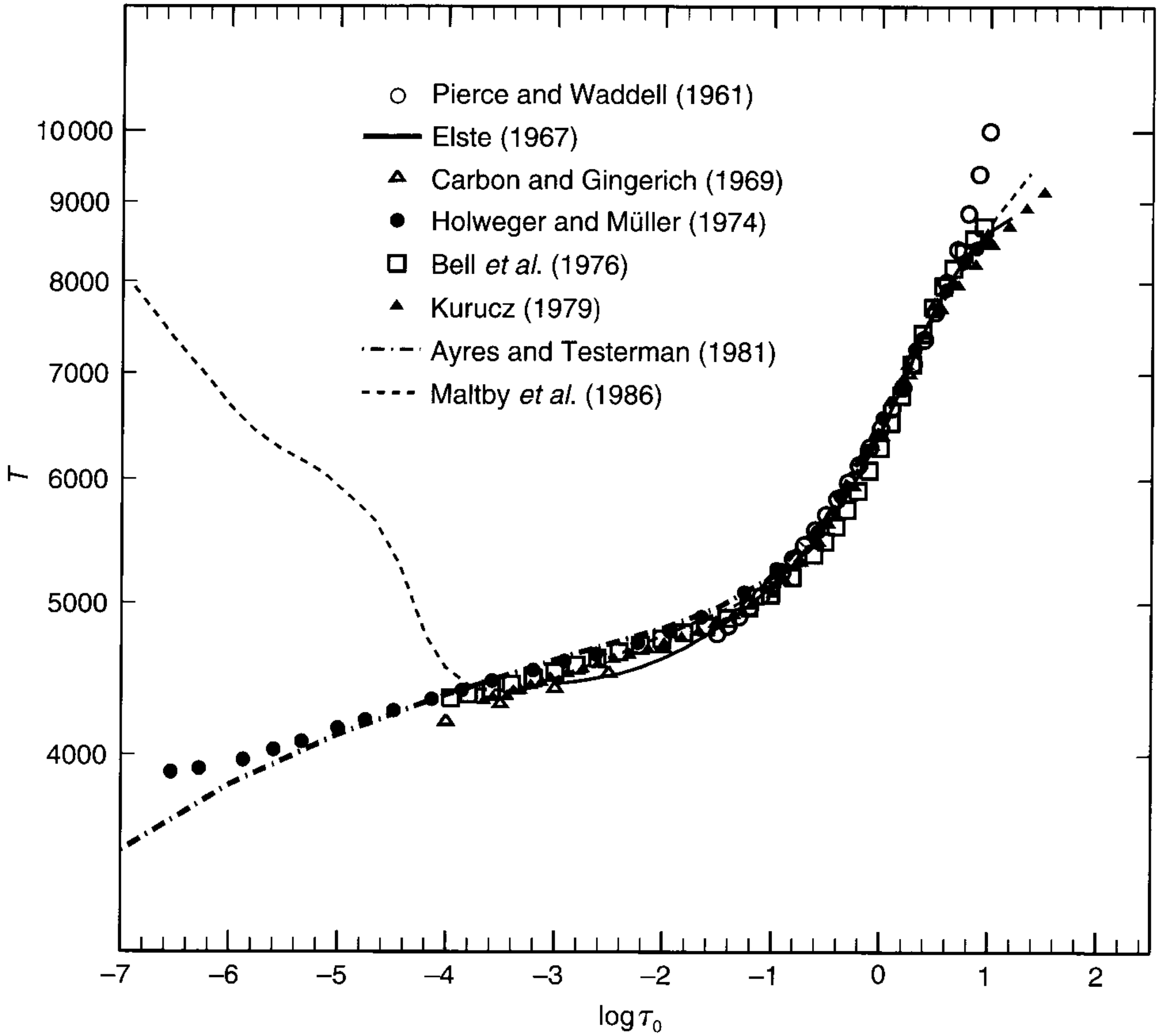

3D hydrodynamical models

Asplund (2005)

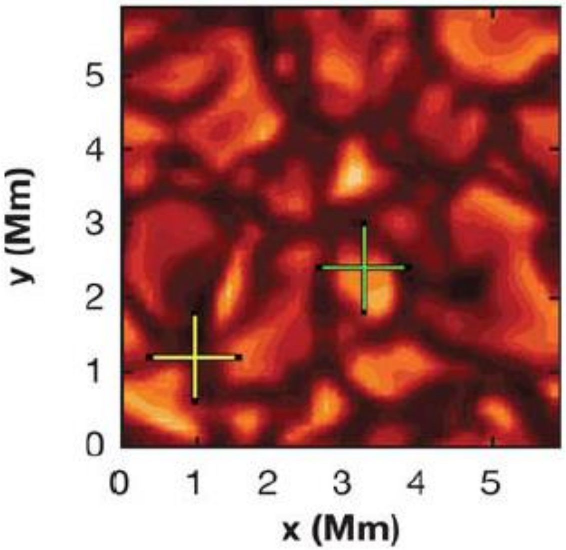

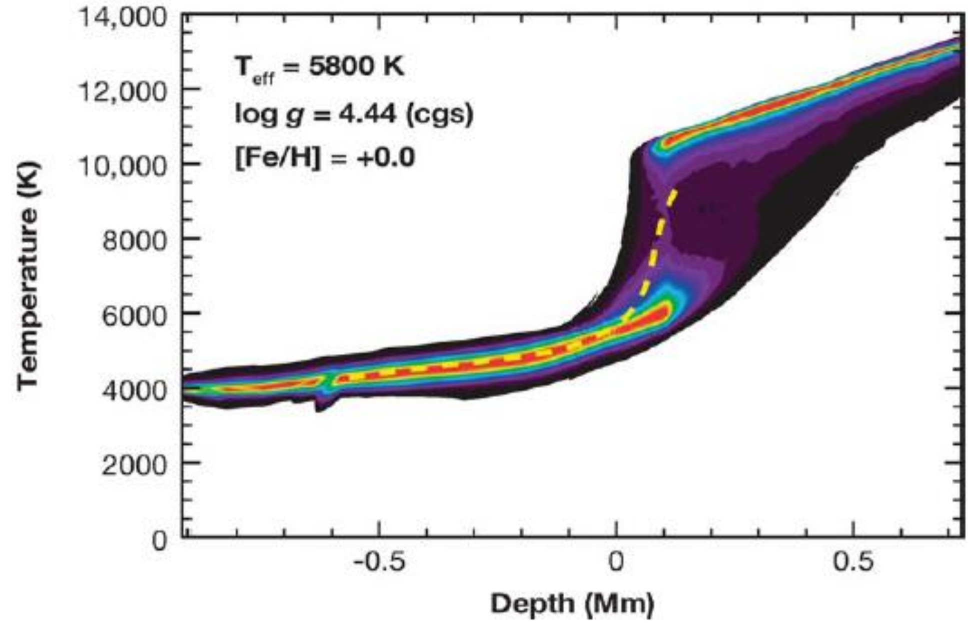

igure 1 Distribution of temperature with height in a 3D hydrodynamical model atmosphere orresponding to the Sun (Asplund et al. 2000b) with *warm colors* denoting an abundance f gas and *cold colors* a shortage of gas at those temperatures. Note the shortage of gas with temperature between 6000 and 10,000 K owing to the very rapid cooling in upflowing aterial as it starts to become optically thin. The zero-point in height corresponds to average ontinuum optical depth unity. Also shown is the temperature structure of a 1D hydrostatic eoretical MARCS model (Asplund et al. 1997) with otherwise identical input parameters *lashed line*), which illustrates that in the 3D model the gas is close to radiative equilibrium the optically thin layers at solar metallicity.

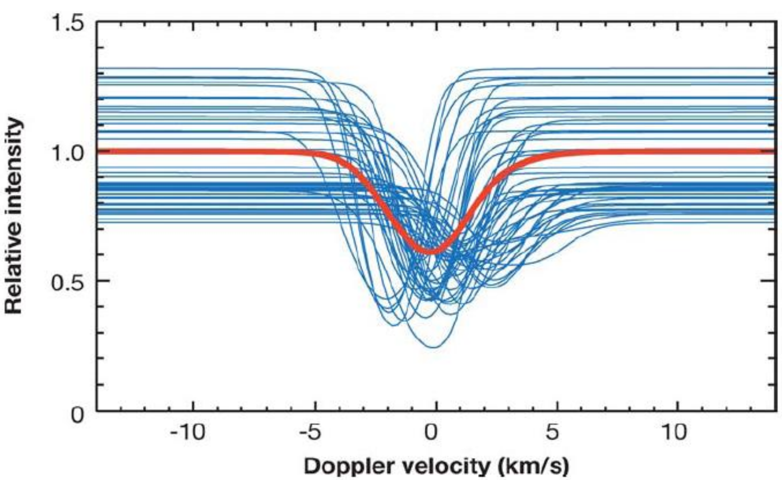

Observational evidence for the 3D effects for the solar model

Asplund et al. (2009)

Wavelength dependence of limb darkening

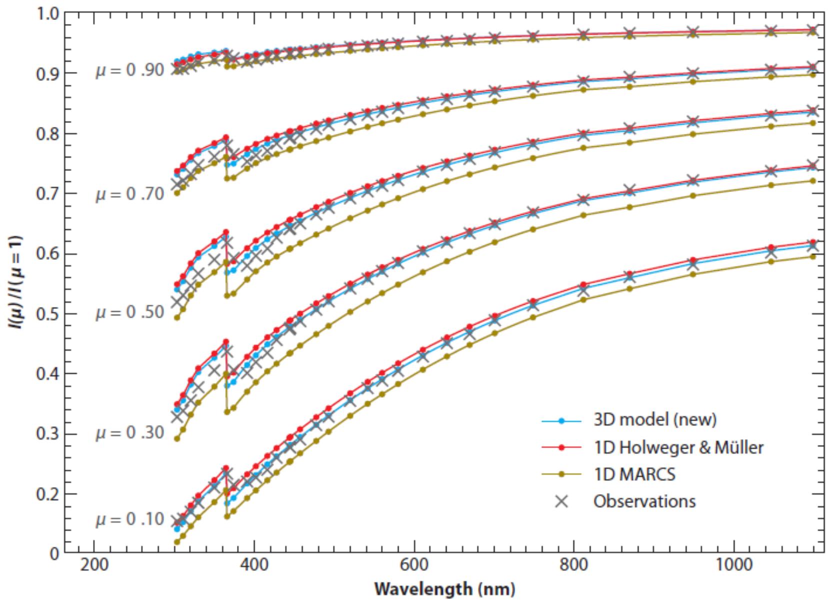

wavelength

Line profile and wavelength shift

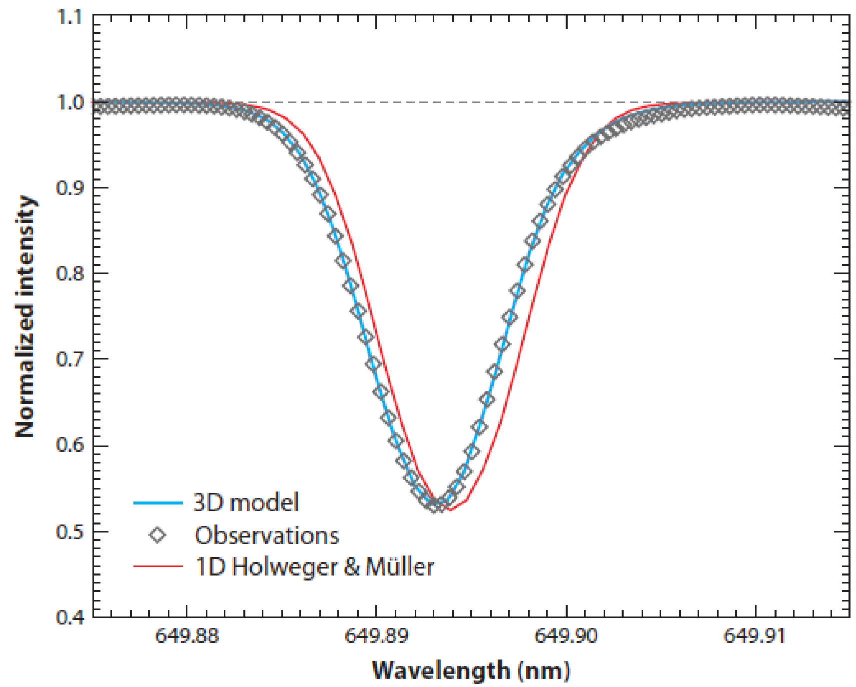

3D models for metal-poor stars

Effect is large at the surface of metal-poor stars

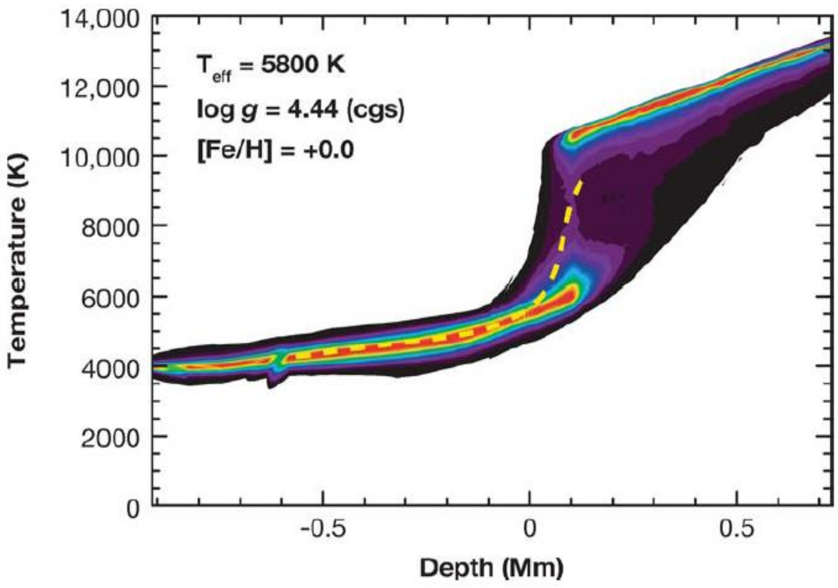

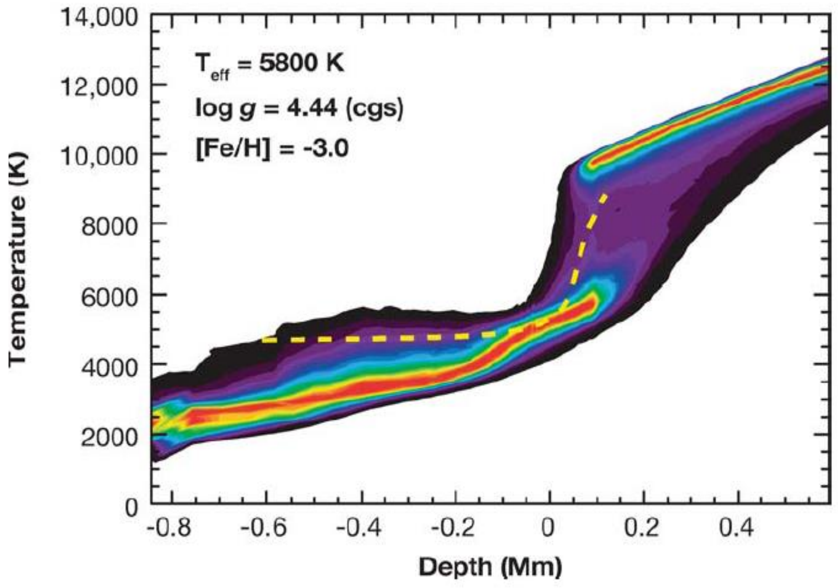

Abundance analysis using model photospheres

- Input data

 -model photosphere (←stellar parameters)

 -chemical composition assumed

 -line data

 (wavelength λ, excitation potential χ,
 transition probability *gf*)

↓

Line opacity / radiative transfer

- output → comparison with observational data

 spectrum / equivalent widths

Feedback to model parameters and chemical composition given as input data if required

Abundance determination

Analysis of equivalent widths

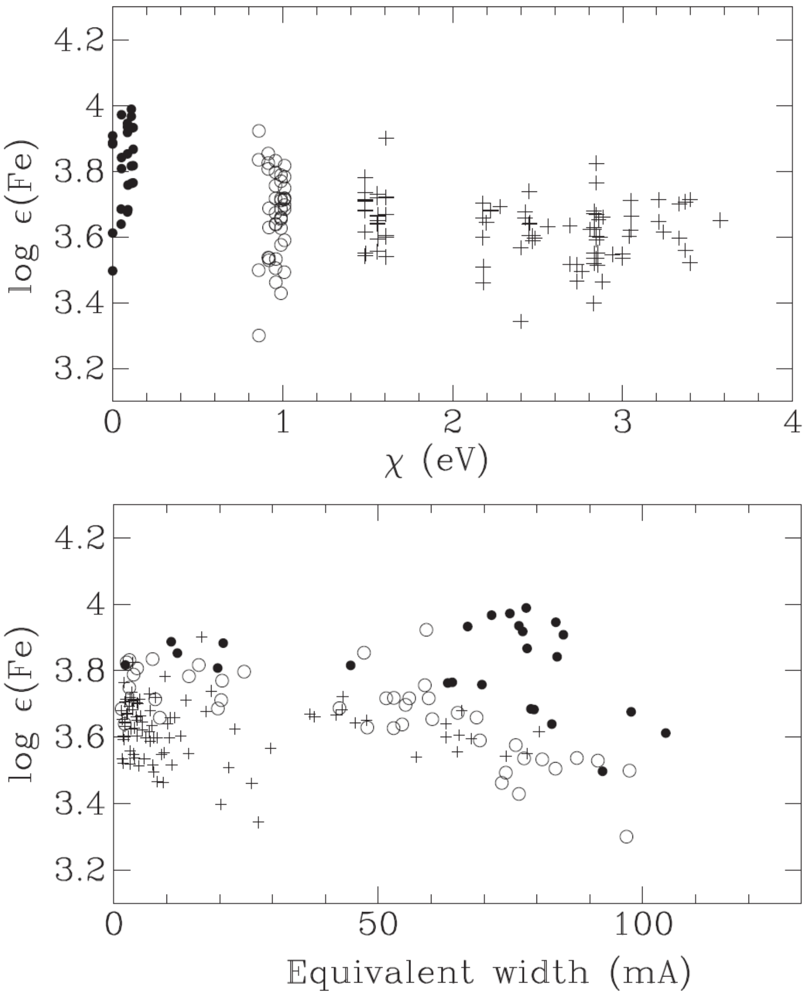

Aoki (2015)

Spectrum synthesis

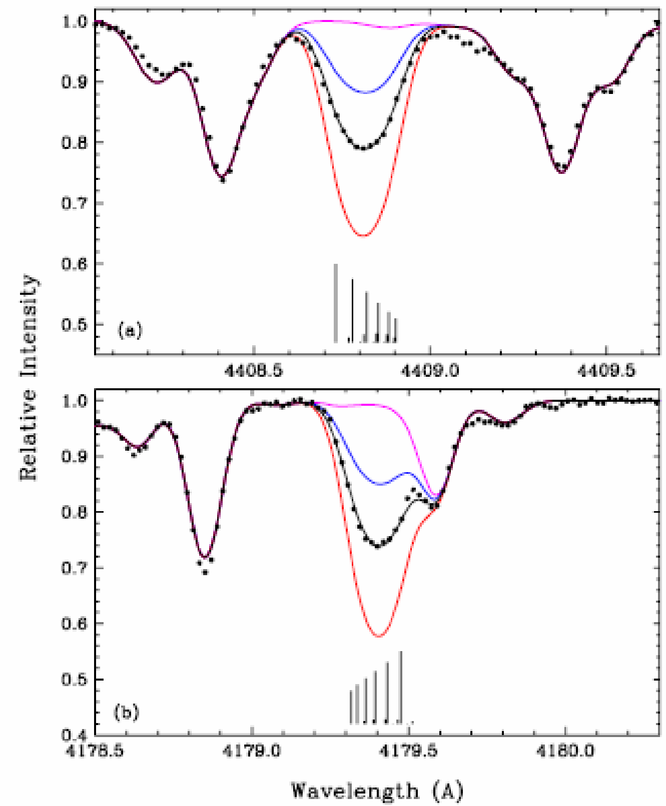

Figure 3. Observed and synthetic spectra in CS 31082−001 of two strong Pr II lines with wide hfs. In each panel, the points represent the observed spectrum. The magenta line is the spectrum computed with no contribution from Pr II; the black line is the best-fitting synthesis (with the Pr abundance given in Table 6); and the red and blue lines are the syntheses computed with Pr abundances altered by ±0.3 dex from the best value. The vertical lines have been drawn at the bottom of each panel to indicate the wavelengths and *relative* strengths (arbitrary overall normalization) of the hyperfine components that comprise the Pr II transitions.

Sneden et al. (2009)

Error sources in abundance analyses

- Noise in observed spectrum (S/N), error in measurement of equivalent widths (→ random error)
  →estimate from S/N, fitting error etc.
- Error in line transition probability (random error?)

- Incompleteness of model photosphere (→systematic?)
- Incompleteness of spectrum calculation (NLTE effects etc.) (→ systematic for each line, but depends on lines used)
- Uncertainty of stellar parameters
  estimates from spectral analysis →random + systematic
  independent estimates (e.g. color index)
  → random + systematic

- Uncertainty in solar abundances used to derive abundance ratios ([X/Fe])

Errors in abundance analyses

- **Uncertain case:**
  - -derived only from strong absorption features
  - -derived from species in minor ionization stage
    - ex. Fe abundances from neutral Fe in solar photosphere
  - -derived from high excitation lines (minor population)

- **Robust case:**
  - -abundance ratios of two elements derived from the same ionization stage.
    - e.g. Mg/Fe from neutral Mg and Fe

Avoiding errors by differential analysis

Differential analysis: deriving abundance ratio with respect to a standard star (ex. the Sun)

- **Noise in observed spectrum (S/N)、error in measurements of equivalent widths**
  (→unavoidable)
- **Error in transition probability**
  →avoidable by using the same line
- **Incompleteness of model photospheres**
  →(mostly) avoidable for the same type of stars
- **Incompleteness of spectrum calculations**
  →(mostly) avoidable by using the same line for the same type of stars
- **Uncertainty of stellar parameters**
  →avoidable for the systematic components

Differential analysis for “solar twin” stars

Melendez et al. (2009)

Observations and Analysis (1)

- Targets:
 -11 solar twins (no planet information)
 -10 solar analogs (with and without giant planets)
- Planets are not well searched for solar twins, while the solar analogs are selected from planet survey.
- 6.5m Magellan telescope and MIKE (E=65,000)
 + Keck/HIRES for one object

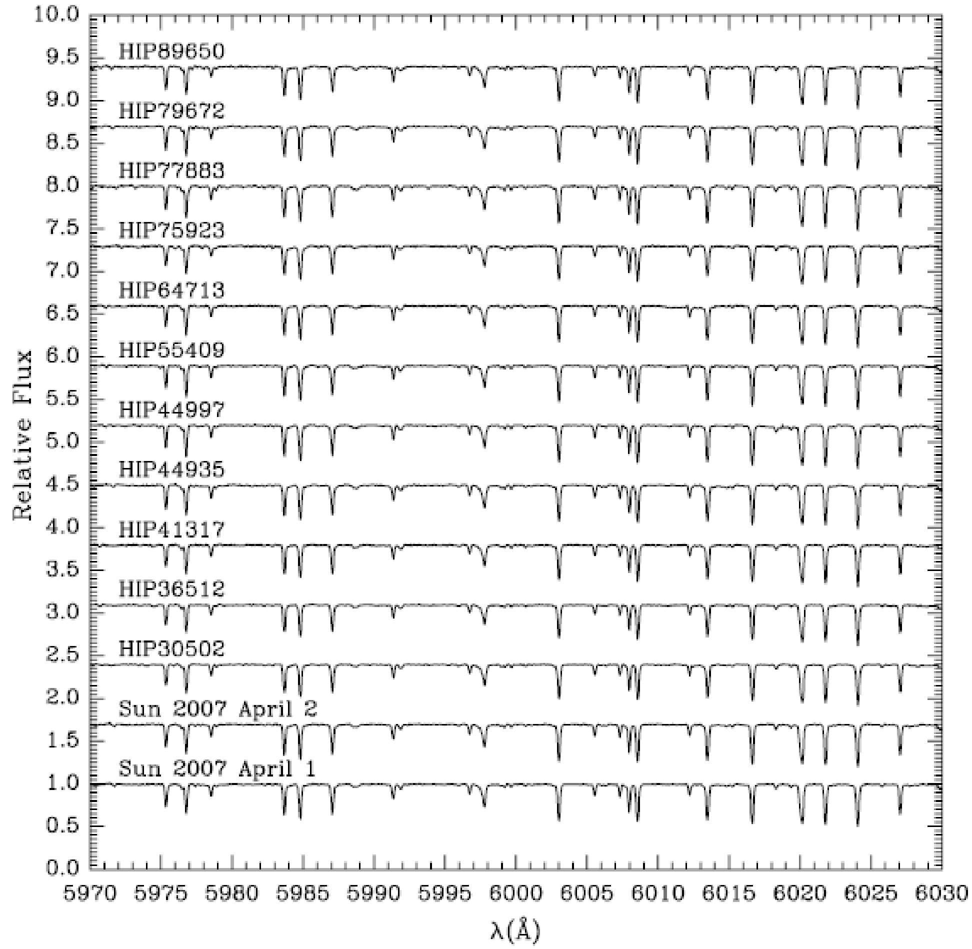

Differential analysis for "solar twin" stars

Melendez et al. (2009)

Observations and Analysis (2)

- A "model independent analysis": direct comparison of line EWs between Sun and a star for different excitation potential and elements.
- Analysis with models are also made.
- Parameters:

-Effective temperatures ($T_{\rm eff}$) from excitation equilibrium

-Surface gravity (log g): ionization equilibrium of Fe I/Fe II

Solar twins have $T_{\rm eff}$ within 75K, log g within 0.10dex and [Fe/H] within 0.07dex.

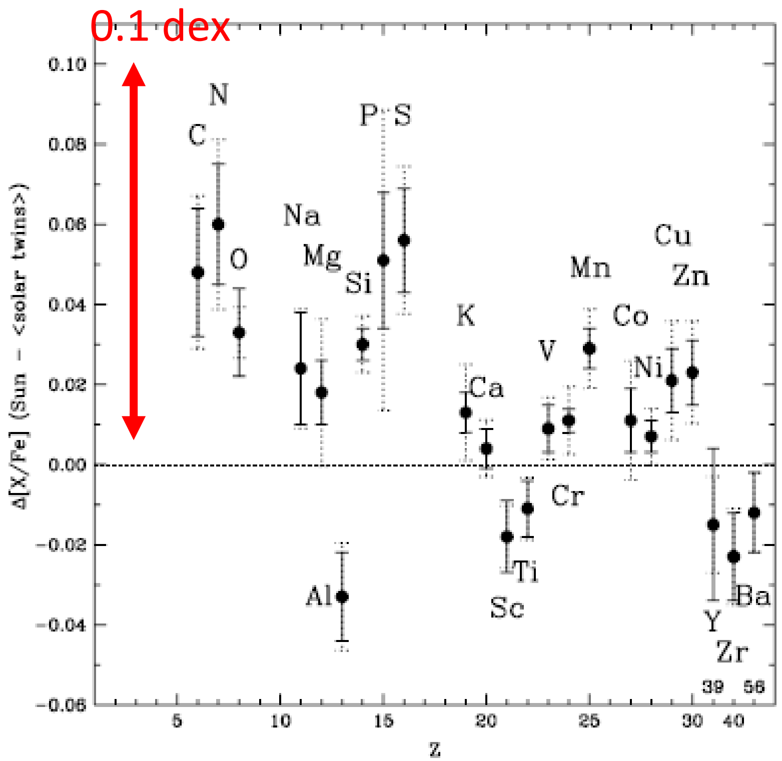

Figure 2. Differences between [X/Fe] of the Sun and the mean values in the solar twins as a function of atomic number Z. For clarity, the elements Y (Z = 39), Zr (Z = 40), and Ba (Z = 56) have been included after Zn. Observational 1σ errors in the relative abundances (including observational errors in both the Sun and solar twins) are shown with dotted error bars, while the 1σ errors in the mean abundance of the solar twins are shown with solid error bars.

Data driven approach for abundance measurements

Example: Ness et al. (2015) for SDSS/APOGEE data

- Generative models for different $T_{\rm eff}$, log g, [Fe/H] from reference objects (~500 stars) in clusters
- Determining $T_{\rm eff}$, log g, [Fe/H] of survey objects (~50,000 stars) using the generative models

Spectrum of reference objects with regions sensitive to $T_{\rm eff}$, log g, [Fe/H]

Sensitivity of the spectra to $T_{\rm eff}$, log g, [Fe/H]

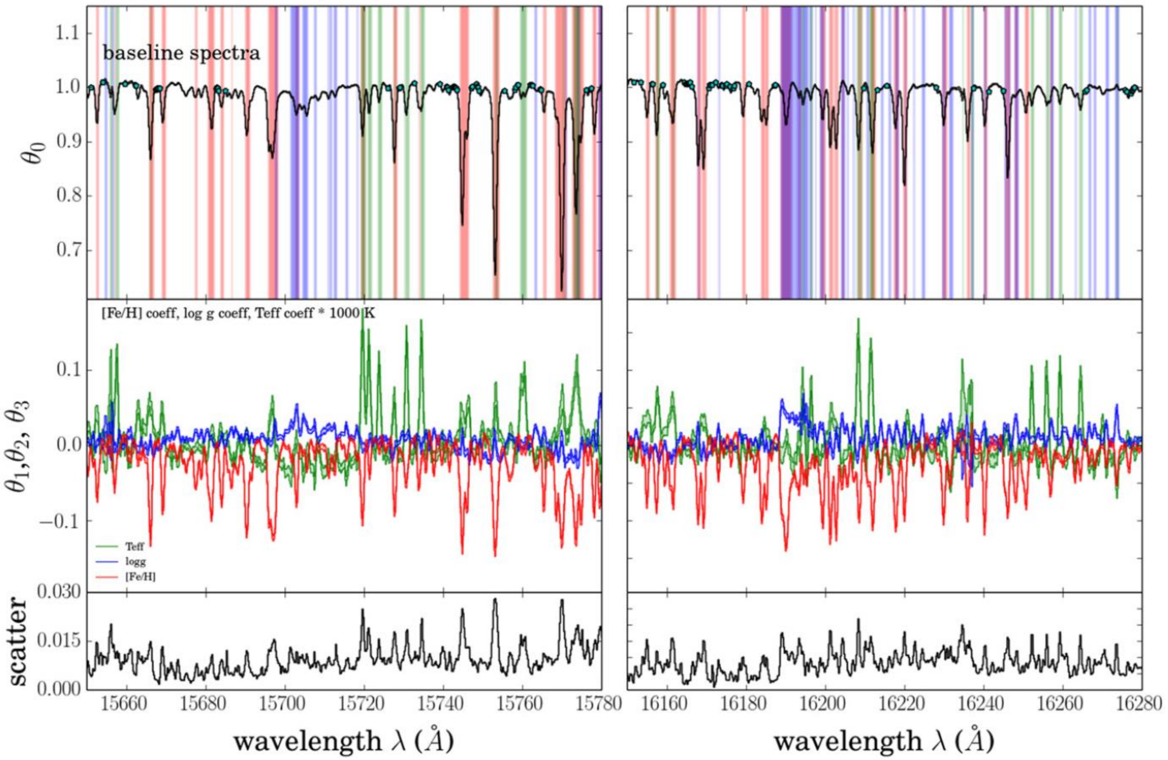

Surface abundances of stars

Composition in the cloud from which the star formed +modification by internal mixing

- **Solar-type stars: composition is homogeneous in the surface convection zone**

- **Chemically peculiar stars: having very thin surface convection zone (+ having strong magnetic field?)**

- **Red giants/supergiants: affected by mixing with products of internal nucleosynthesis (ex. CNO cycle)**

- **Mass accretion from companion can be effective in binary systems**

Chemically peculiar stars

Ex. objects showing large excesses of heavy elements

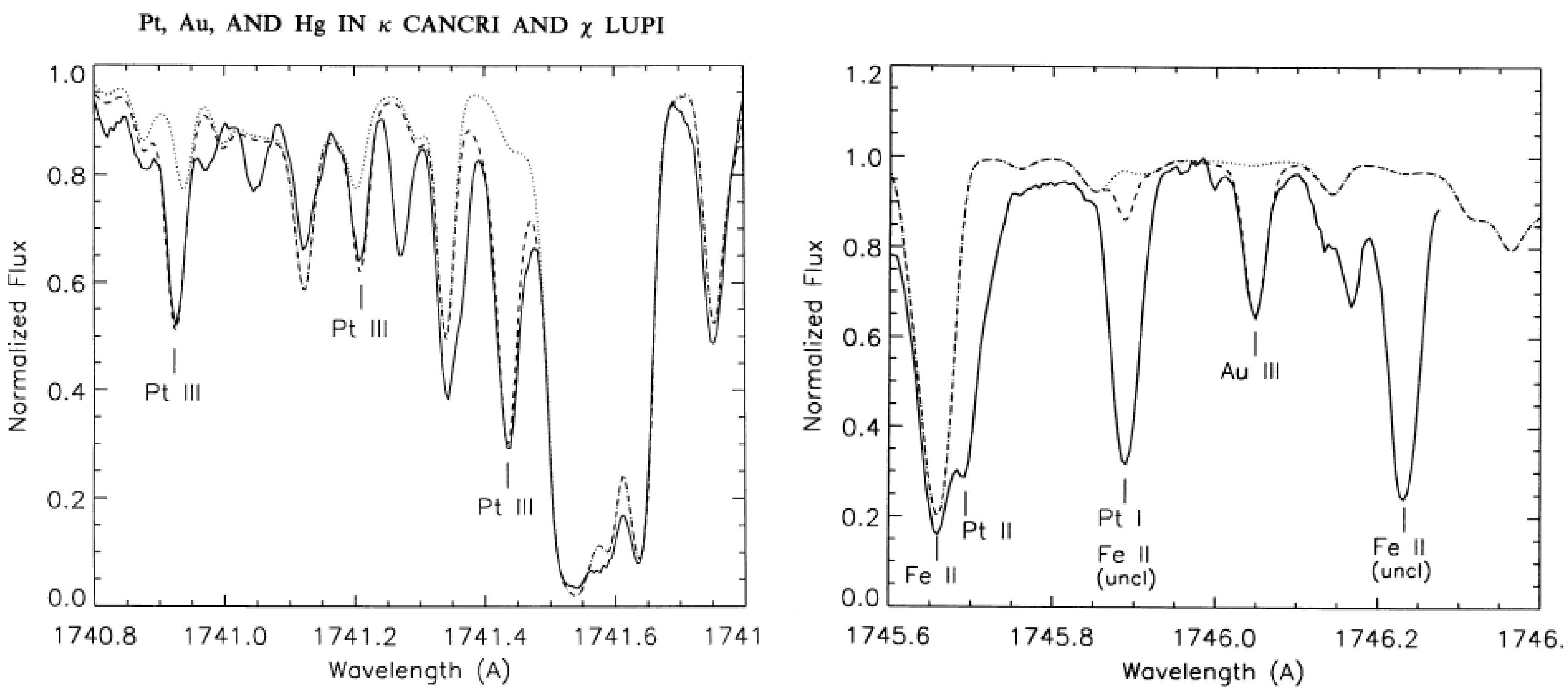

Wahlgren et al. (1995)

Which elements can be measured?

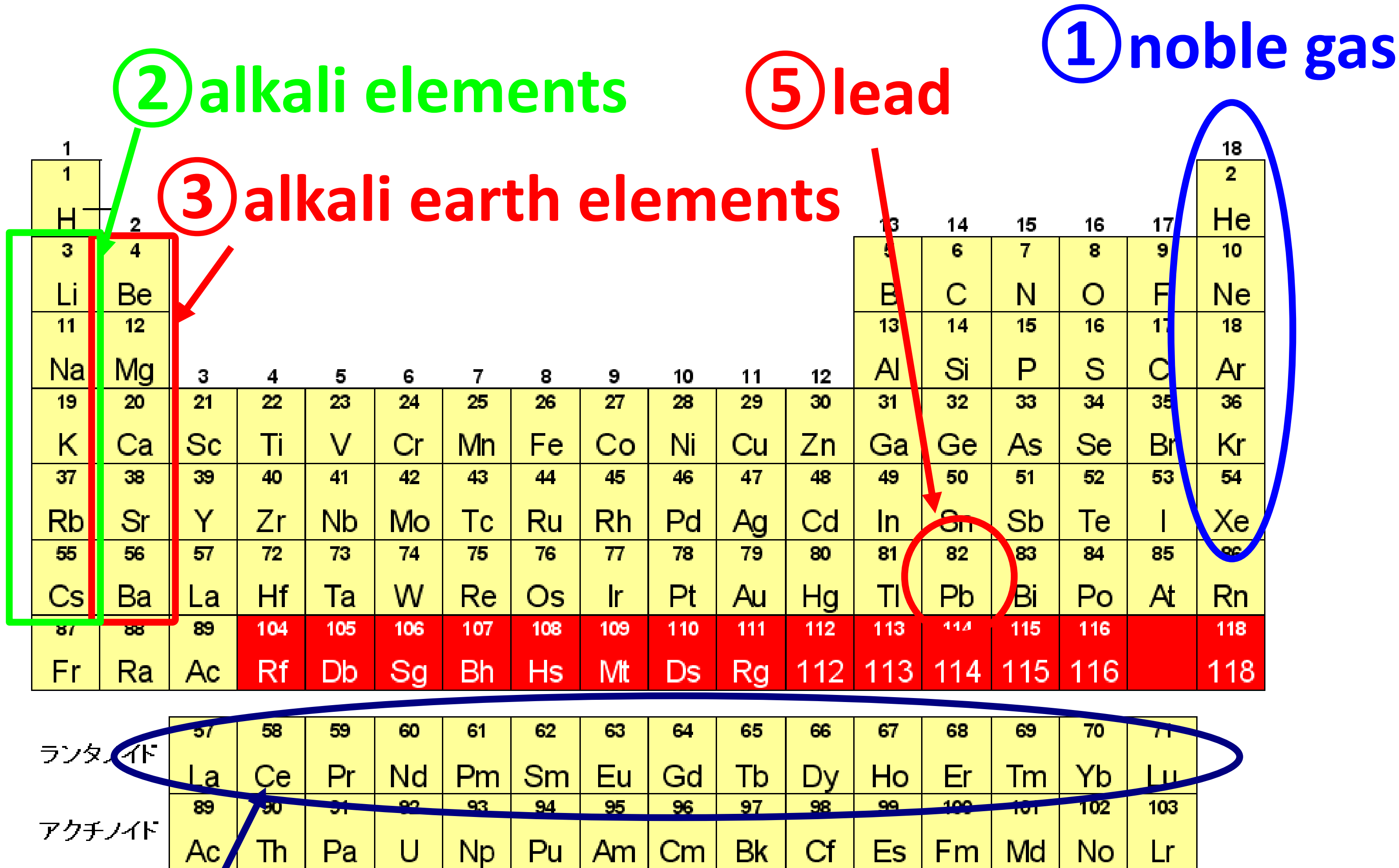

図1　元素の周期表

［資料提供］永 目 諭 一 郎　氏

Which elements can be measured?

①noble gas: Ar, Kr,...
No useful spectral features in the optical range measurable for cool stars. Emission lines are detectable in planetary nebulae.

②alkali elements: Na, K, Rb, Cs
Mostly ionized in stellar atmosphere. Remaining neutral Na and K have however strong doublet features. Rb and Cs are detectable only in very cool stars.

③alkali earth elements: Mg, Ca, Sr, Ba
Singly ionized species have strong doublet lines (ex. Ca K lines) and easily detectable even in metal-poor stars.

④lantanides:La, Ce, Pr, Nd, Sm, Eu, Gd, Dy, ...
Many lines of singly ionized stage exist in the optical. Relative abundances are well determined.

⑤lead
Measurable lines exist in the optical range.

Cs absorption lines in brown dwarfs

Brown dwarf GL229B

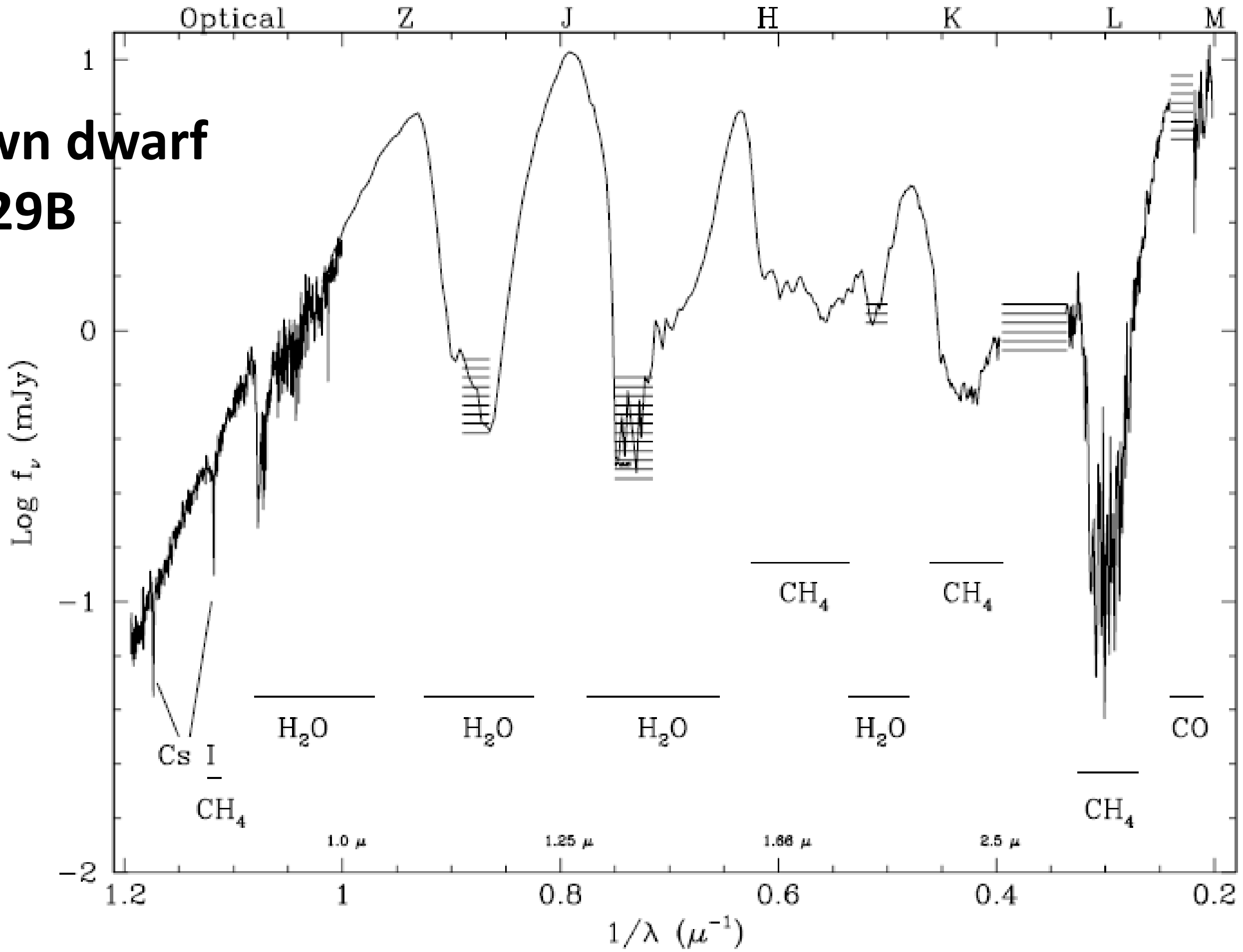

Oppenheimer et al. (1998)

Lantanides abundances determined for "r-process-enhanced" very metal-poor stars

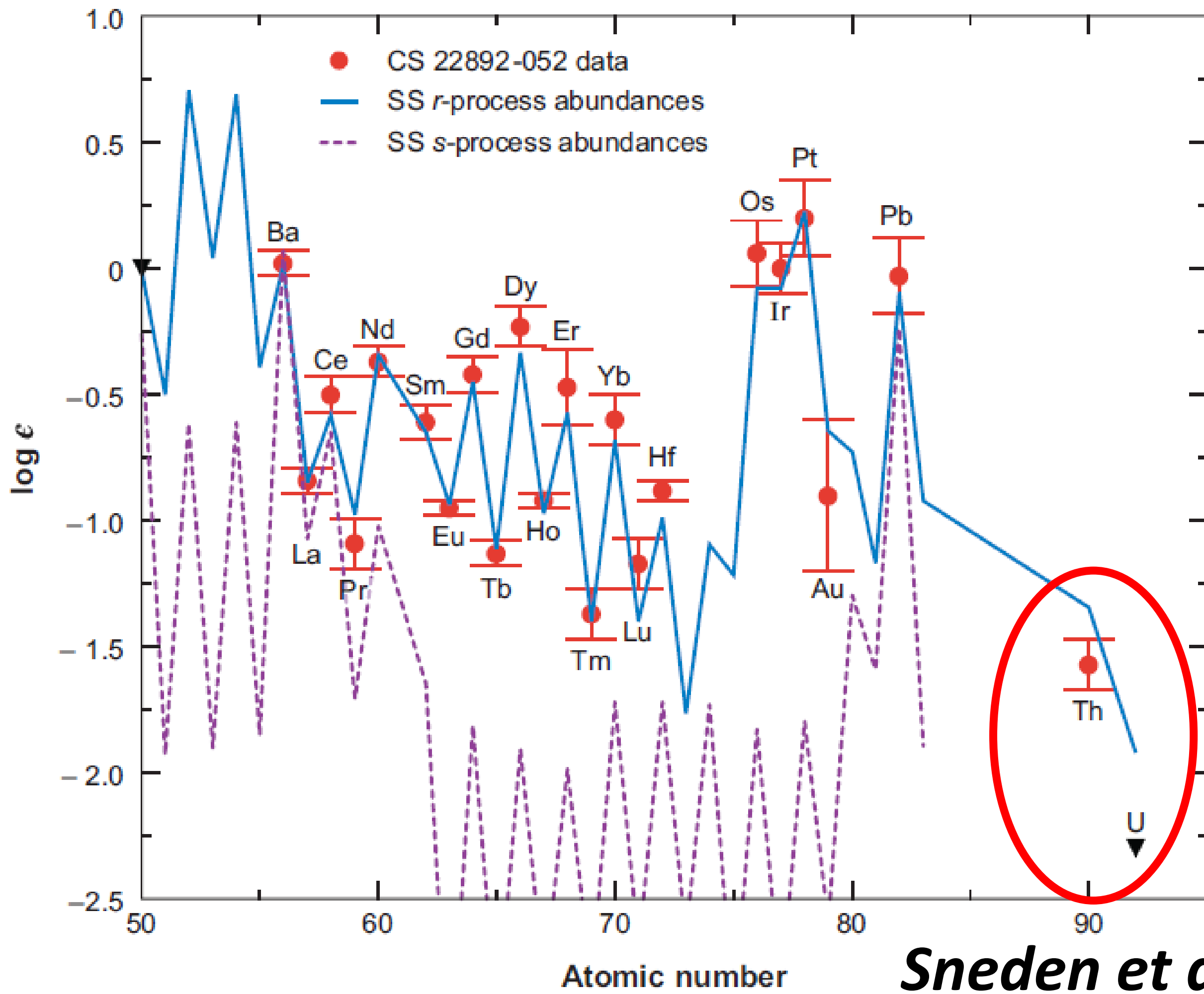

Sneden et al. (2008)

Recent measurements of transition probability for rare earth elements

Experiments have been conducted from astronomical interests

La II: Lawler et al. (2000, ApJ, 556, 452)
Eu II: Lawler et al. (2001, ApJ, 563, 1075)
Tb II: Lawler et al. (2000, ApJS, 137, 341)
Nd II: Den Hartog et al. (2003, ApJS, 148, 543)
Ho II: Lawler et al. (2004, ApJ, 604, 850)
Pt I: Den Hartog et al. (2005, ApJ, 619, 639)
Sm II: Lawler et al. (2006, ApJS, 162, 227)
Gd II: Den Hartog et al. (2006, ApJS, 167, 292)
Hf II: Lawler et al. (2007, ApJS, 169, 120)
Er II: Lawler et al. (2008, ApJS, 178, 71)
Ce II: Lawler et al. (2009, ApJS, in press)
Pr II, Dy II, Tm II, Yb II, Lu II: Sneden et al. (2009, ApJS)
....

Solar abundances

- **Determination of abundances by spectral line analysis (as for stars)**
  - **almost all elements including volatile elements C, N, O, …**
  - **advantage of solar spectral analysis**
    - **very high quality spectrum**
    - **accurate model parameters**
    - **spatially resolved spectra**
- **Determination of abundances from meteorites analysis**
  - **metal abundances**
  - **advantages**
    - **very accurate**
    - **isotope ratios**
- **Solar wind, corona etc.**
  - **noble gases He, Ne, Ar, …**

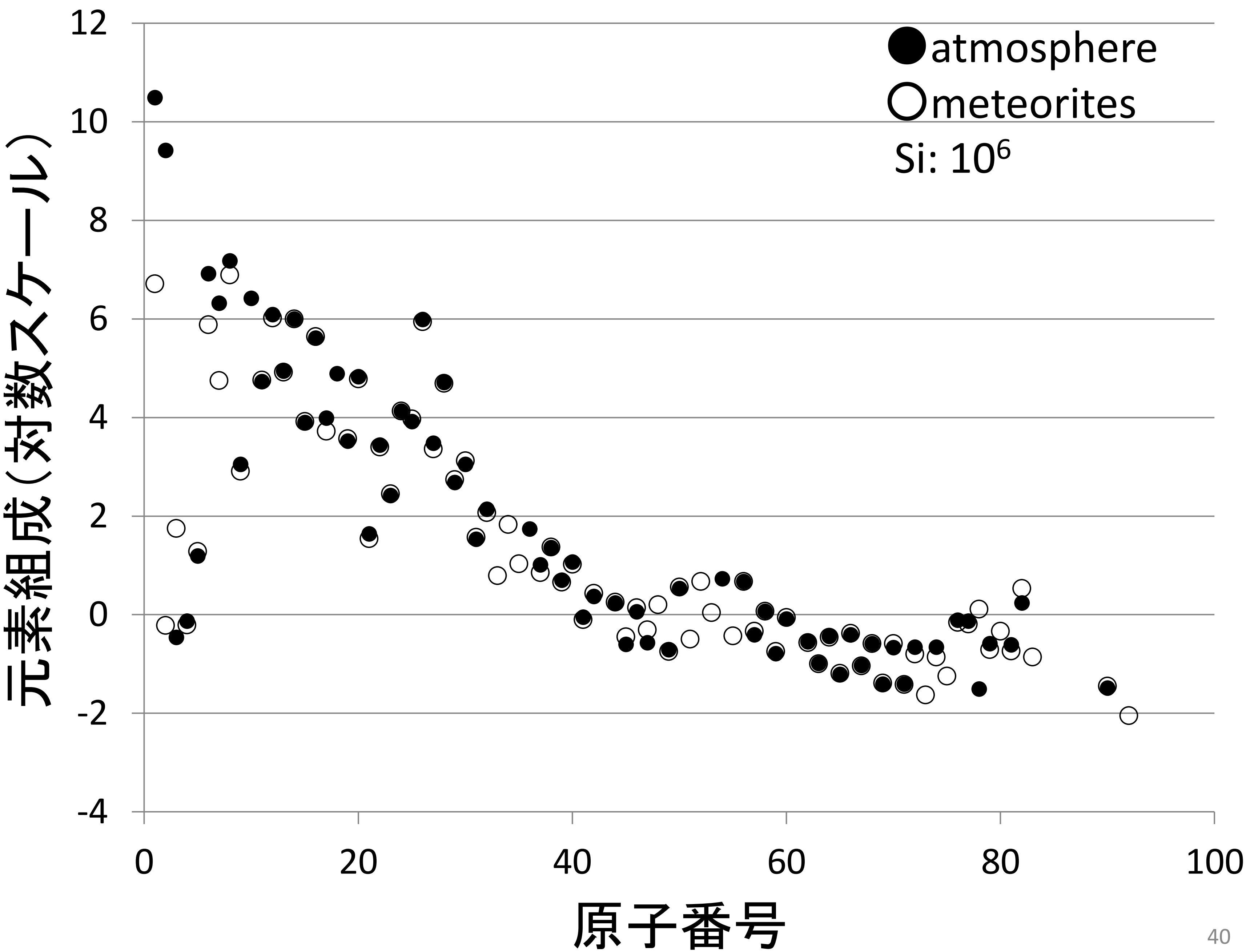

atmosphere
meteorites
Si: 10^6
元素組成（対数スケール）
原子番号
12
10
8
6
4
2
0
-2
-4
0
20
40
60
80
100

Analysis and compilation of solar abundances

- **Anders & Grevesse (1989)**
  - **analysis based on 1D model atmosphere**
  - **meteorite analysis**

- **Asplund et al. (2009)**
  - **analysis based on 3D model atmosphere**
  - **updated atomic data**
  - **meteorite analysis**

Cf. 理科年表「宇宙の組成」

Iron (Fe) abundance of the Sun
$\log \varepsilon = 7.50$ or 7.67

Analysis of new Fe I and Fe II lines

Blackwell et al. (1995a,b), Holweger et al. (1995)

- **Low excitation lines → high Fe abundance**
- **New & more complete line data (Fe I and Fe II)**
  → low value

Cf. Fe II is dominant in solar atmosphere

CNO abundances

Re-estimate of blending

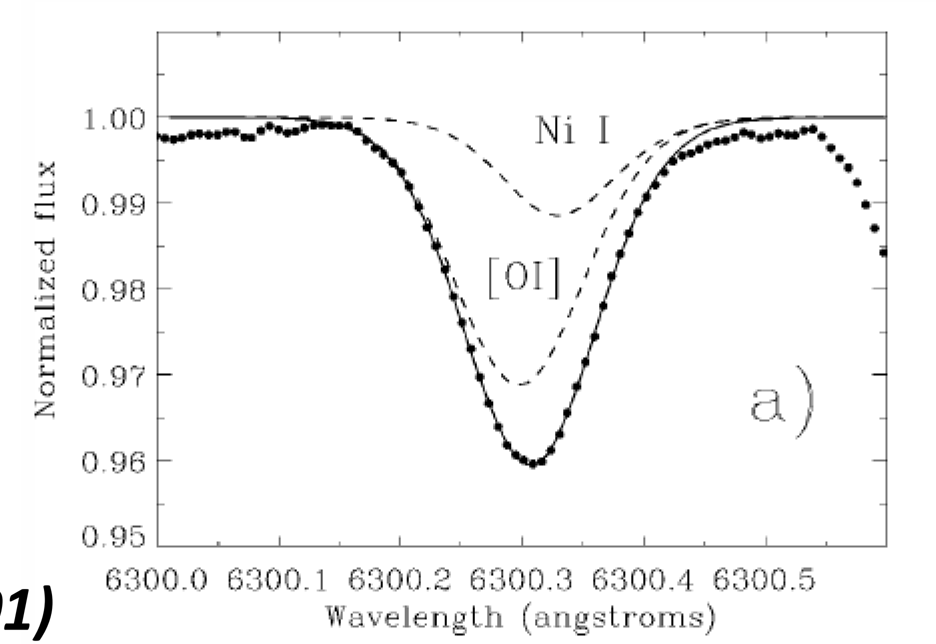

[O I] spectrum
Allende-Prieto et al. (2001)

3D effect on molecular spectra

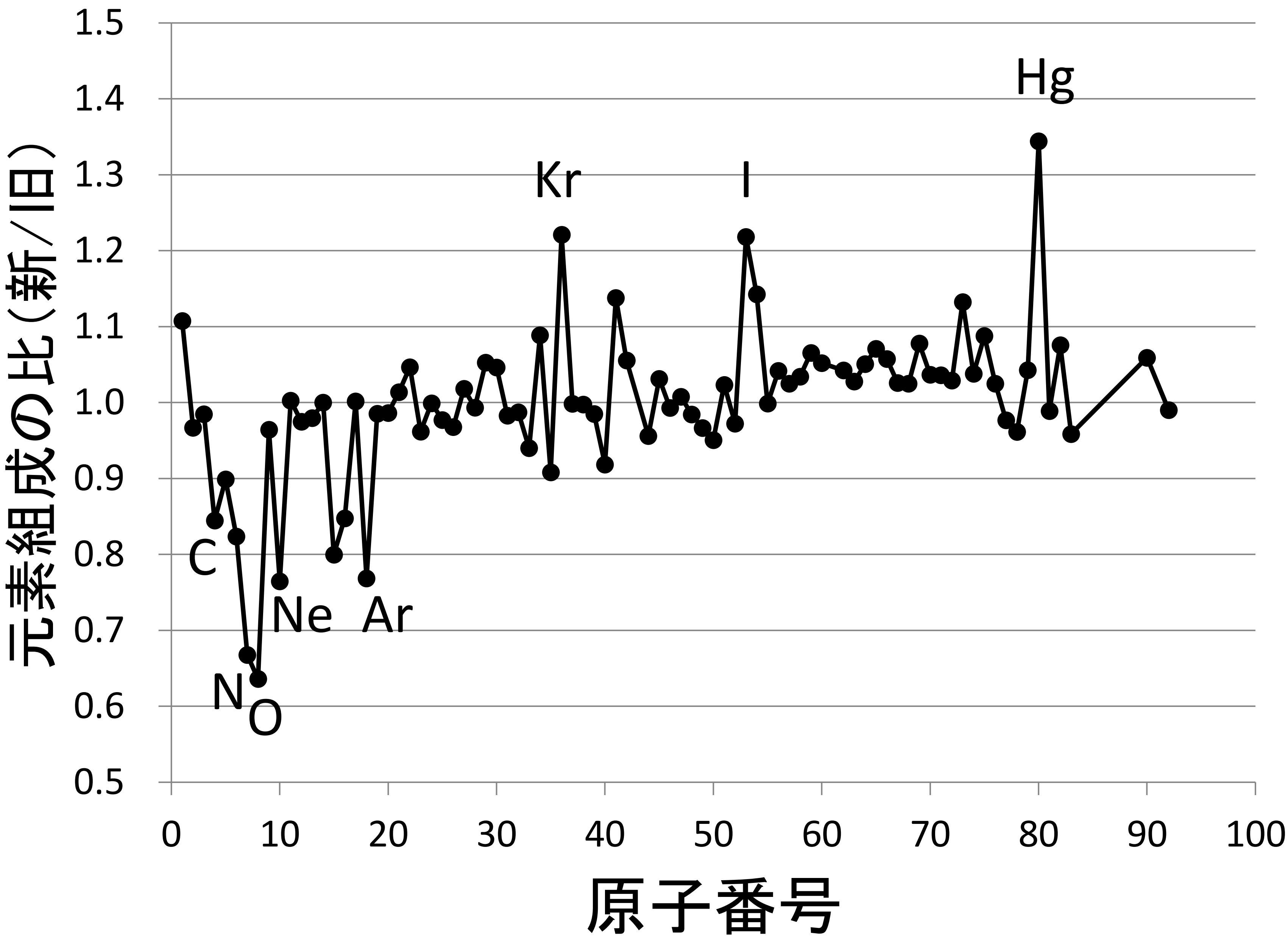

元素組成の比（新/旧）
1.5
1.4
1.3
1.2
1.1
1.0
0.9
0.8
0.7
0.6
0.5
0
10
20
30
40
50
60
70
80
90
100
原子番号
C
N
O
Ne
Ar
Kr
I
Hg

Analysis of solar abundance: s-process v.s. r-process

Burris et al. (2000)

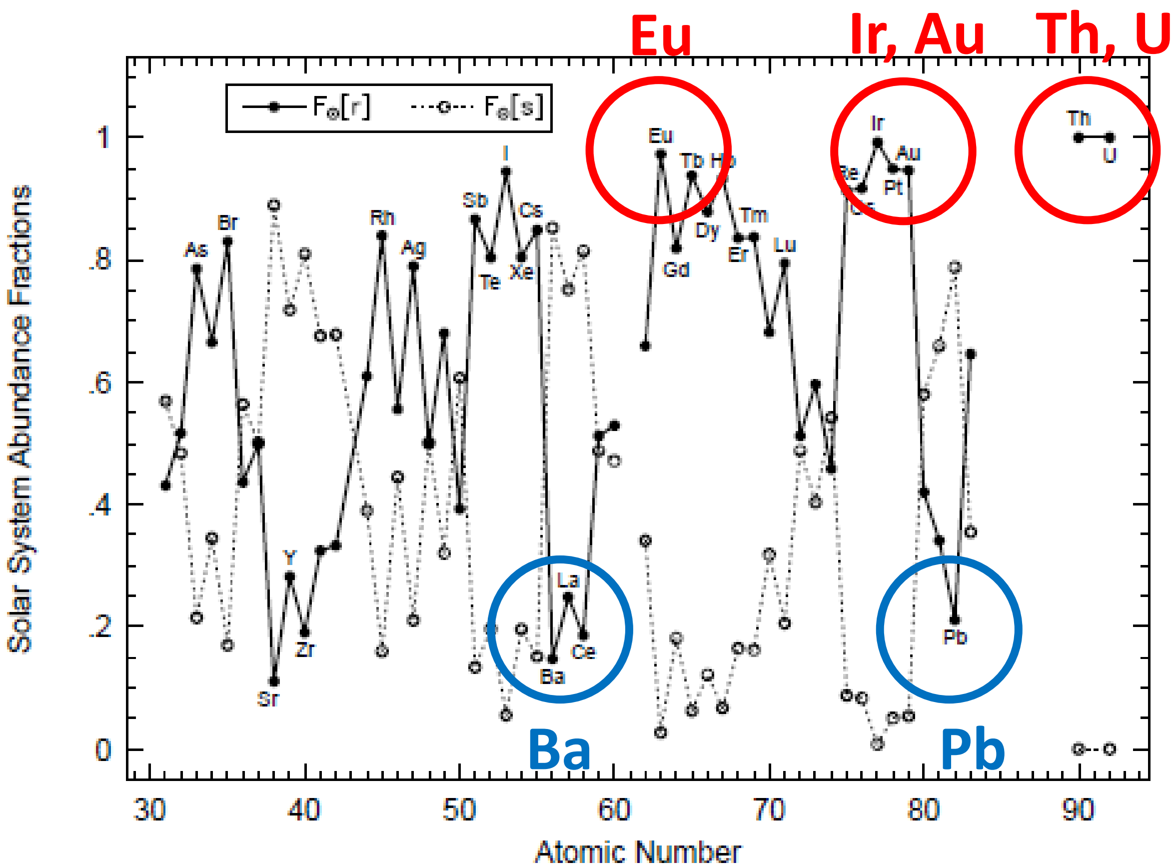

Isotope ratios

- **Isotopes: having same number of protons but different number of neutrons**

  →same(similar) chemical property, but different mass

- **Spectral lines of isotopes are similar, but wavelengths are slightly different**

  -difference of nuclear mass

  -difference of nuclear spin

Nuclear chart

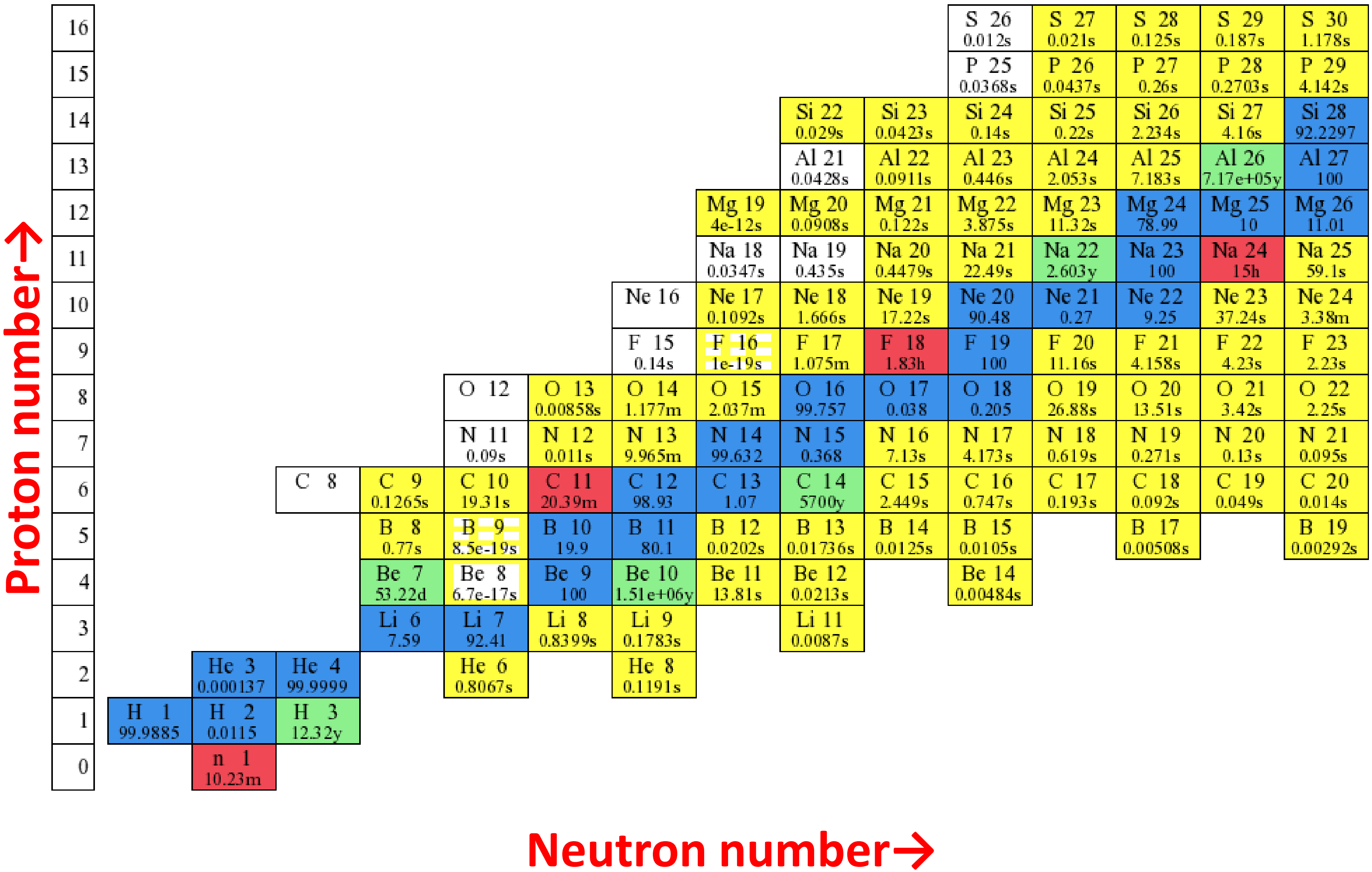

Li isotopes in interstellar matter

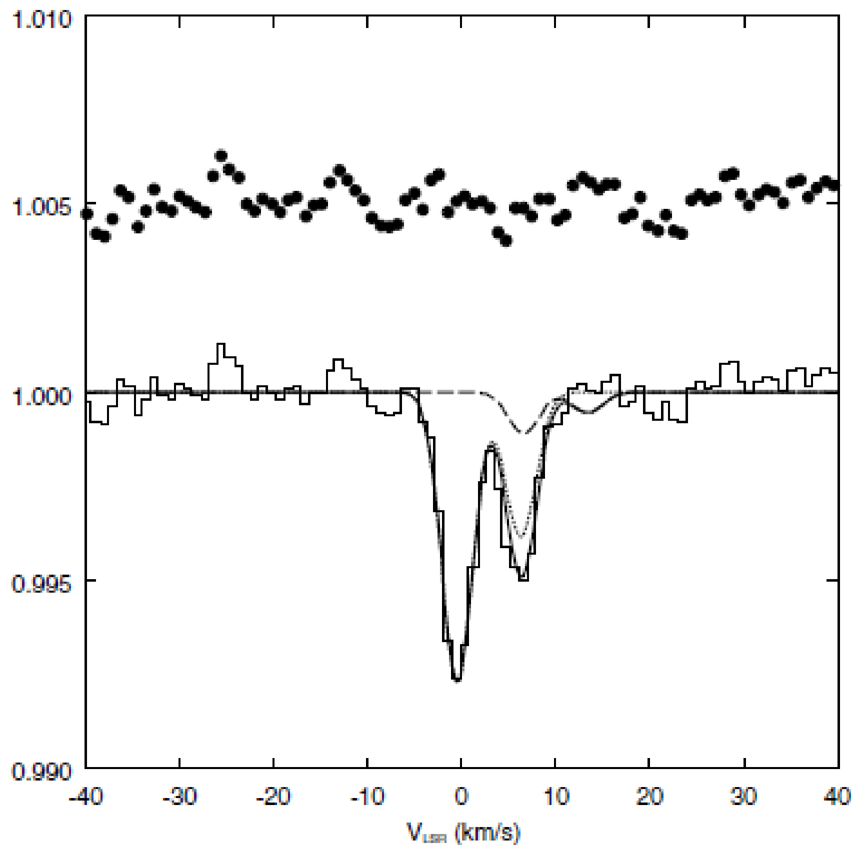

Kawanomoto et al. (2009)

Measurement of isotopes: light elements

^{6}Li measurements for a metal-poor star (1993)

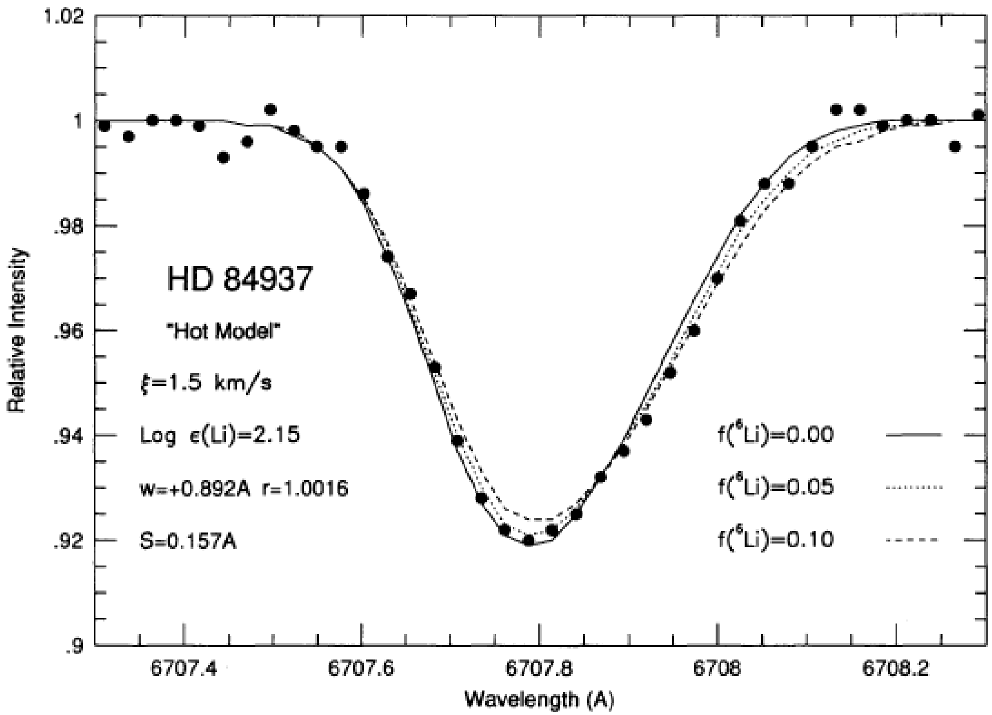

FIG. 13.—Li I line-profile HD 84937 (filled circles are the observed points) with three synthetic spectra (*continuous curves*) generated from a hotter (T_{eff} = 6135 K) model atmosphere. Compared to the best model atmosphere, the Li abundance is increased by +0.03 dex and the smoothing (derived from the Ca I 6162.17 Å line) is increased by +0.004 Å, however, the best estimate for $f(^{6}\mathrm{Li})$ is not changed significantly using this hotter model atmosphere.

Smith et al. (1993)

Measurements by better spectra

Asplund et al. (2006)

ESO/VLT UVES spectra

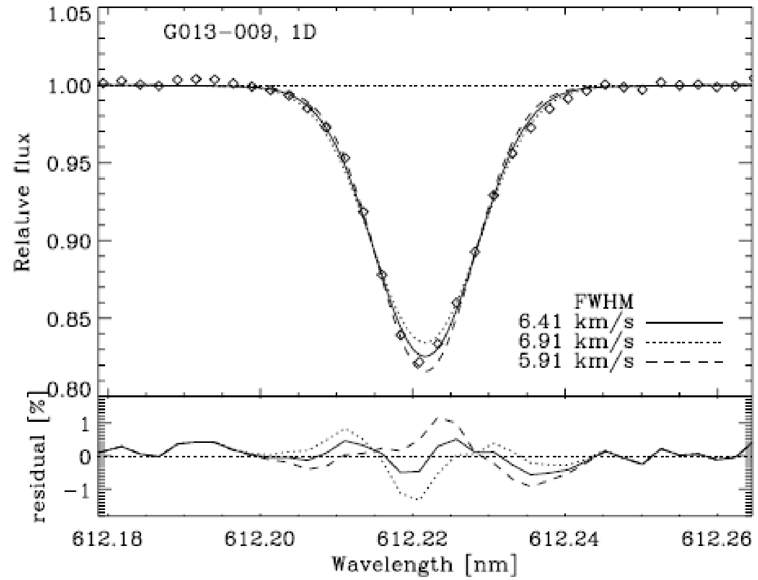

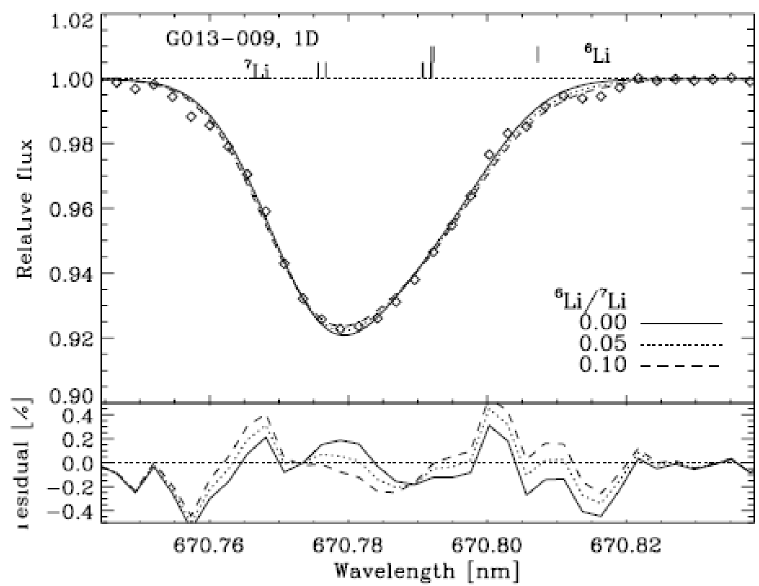

Effects of Internal motion of atmosphere on line profile?

Hinode
JAXA/NASA/PPARC

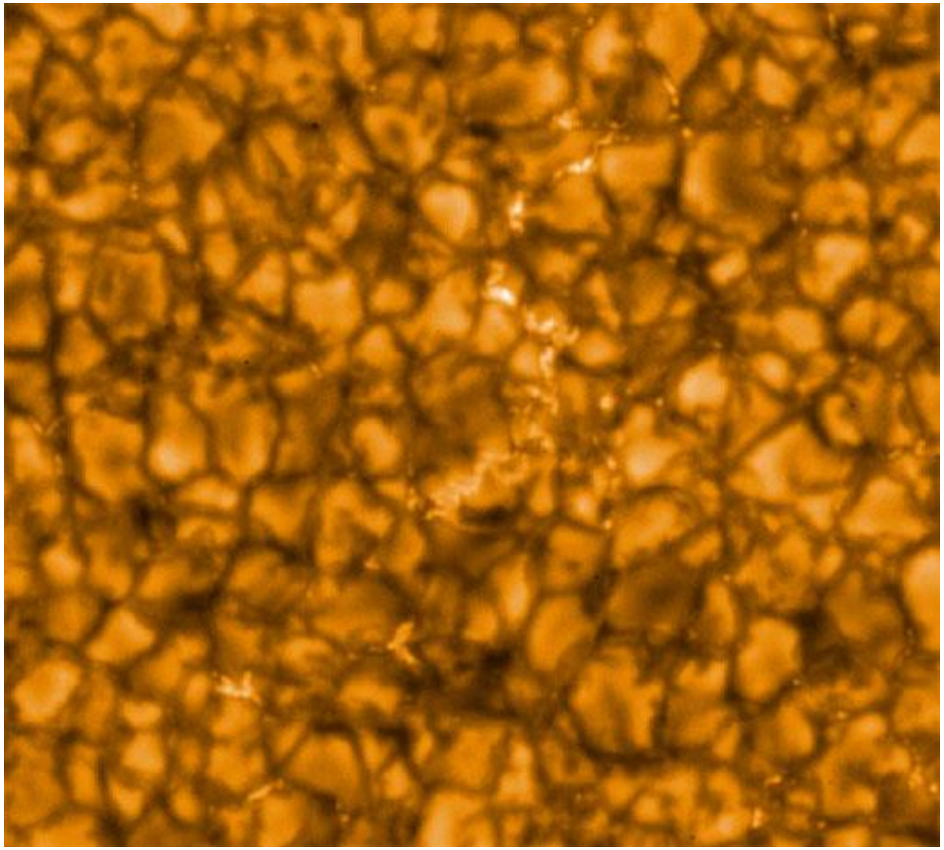

Effects of Internal motion of atmosphere on line profile?

D. Gray (2005)

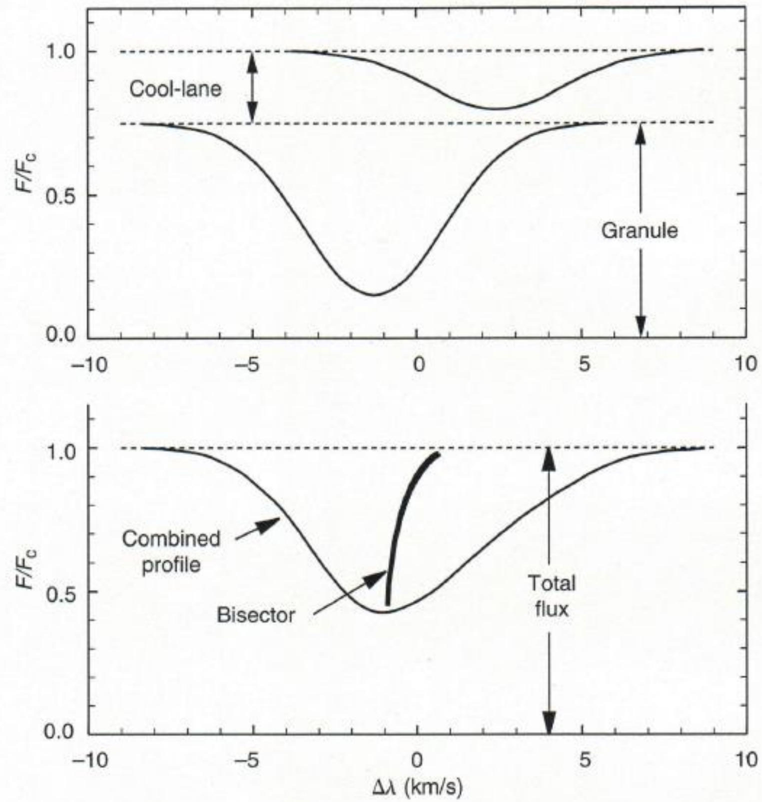

Fig. 17.12. A simple two-stream model helps us visualize how granulation produces asymmetries in lines. At disk center, fall velocities are directed away from us while rise velocities are toward us. The spectrum from the cool falling material alone is shown at the top. Under it is the profile from the hot rising material. At the bottom is the combined profile, i.e., the sum of the two. The net result is a profile that is mostly blue-shifted with a depressed red wing. The bisector shows this quantitatively.

Effects of Internal motion of atmosphere on line profile?

(Cayrel et al. 2007)

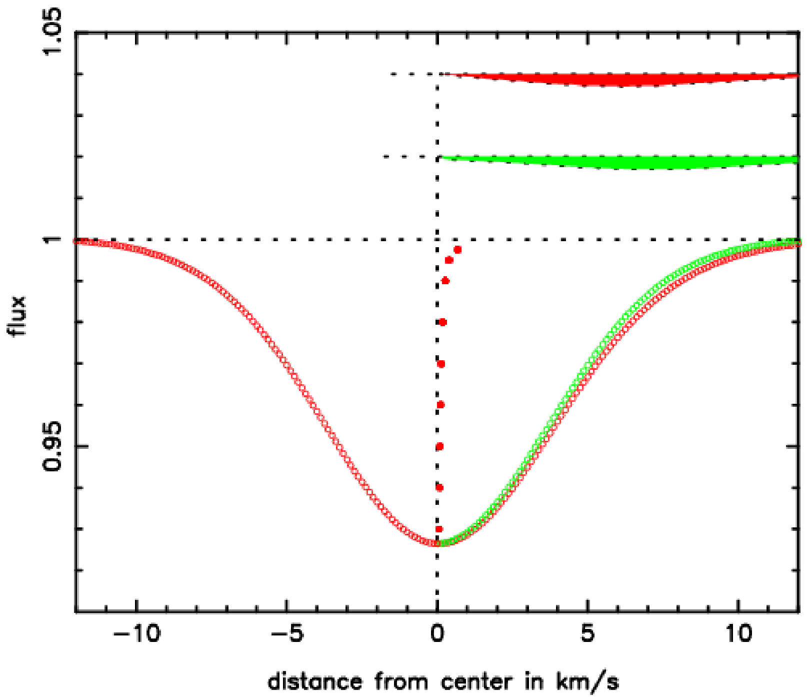

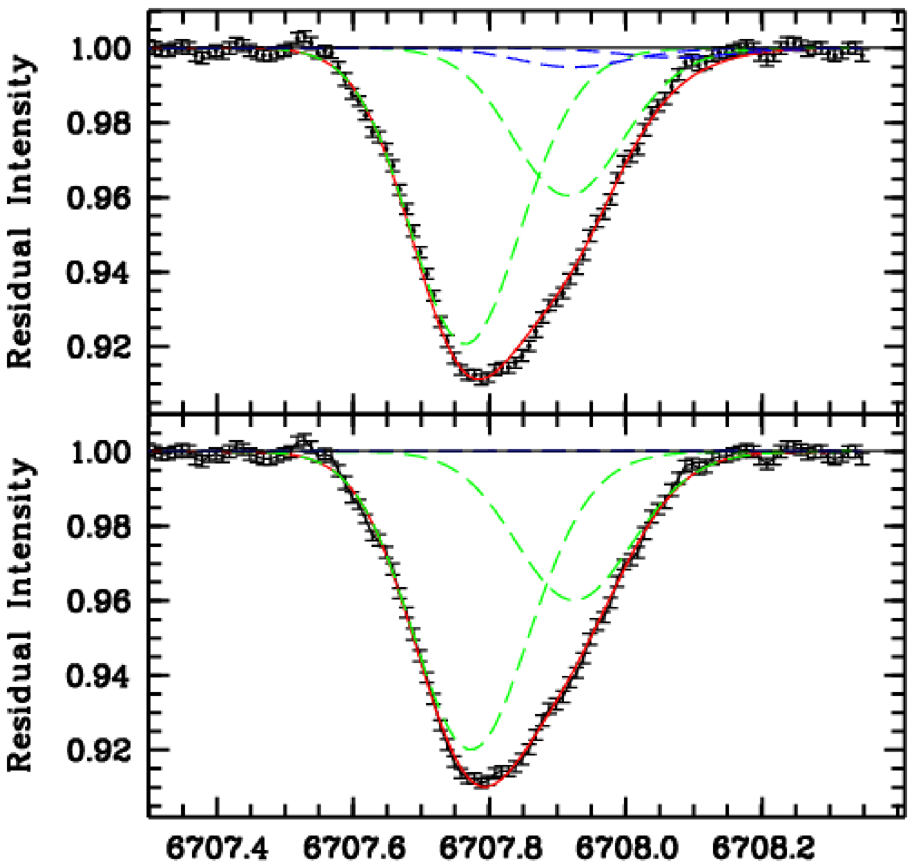

Effects of Internal motion of atmosphere on line profile?

Analysis with 3D atmospheres

Asplund et al. (2006)

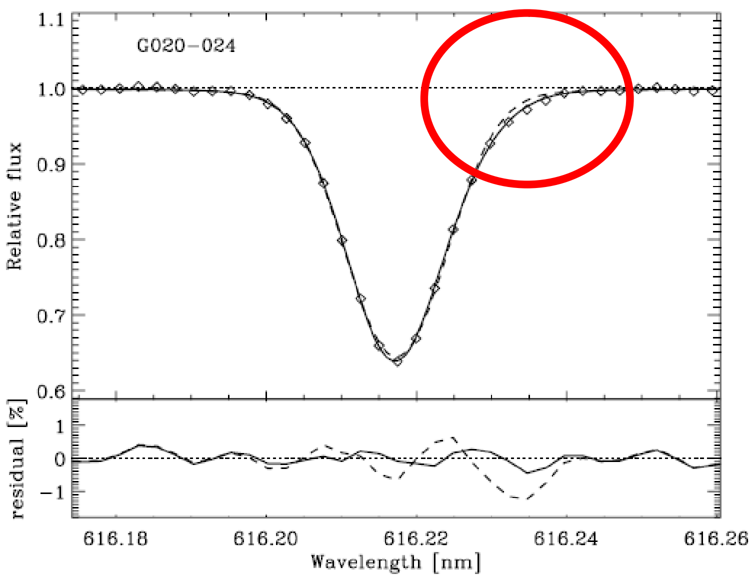

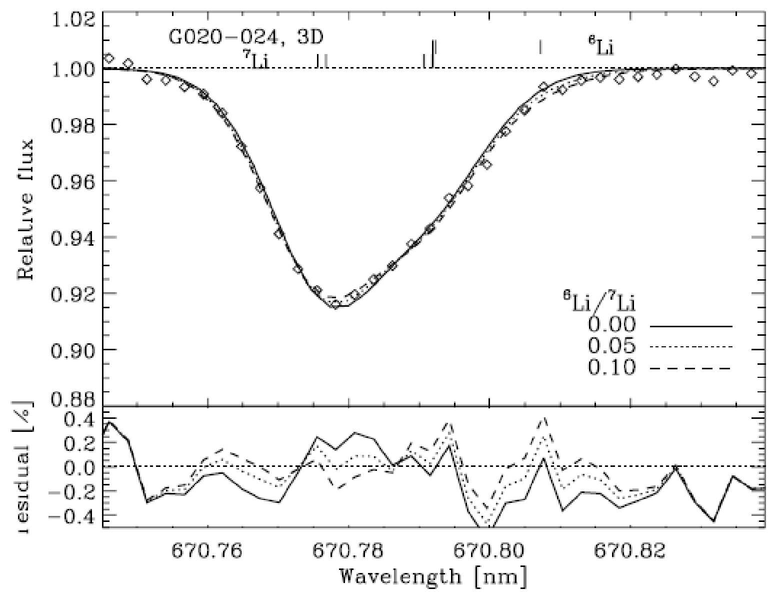

More recent study by Lind et al. (2013)

No detection of 6Li by 3D/NLTE analysis

Lind et al. (2013)

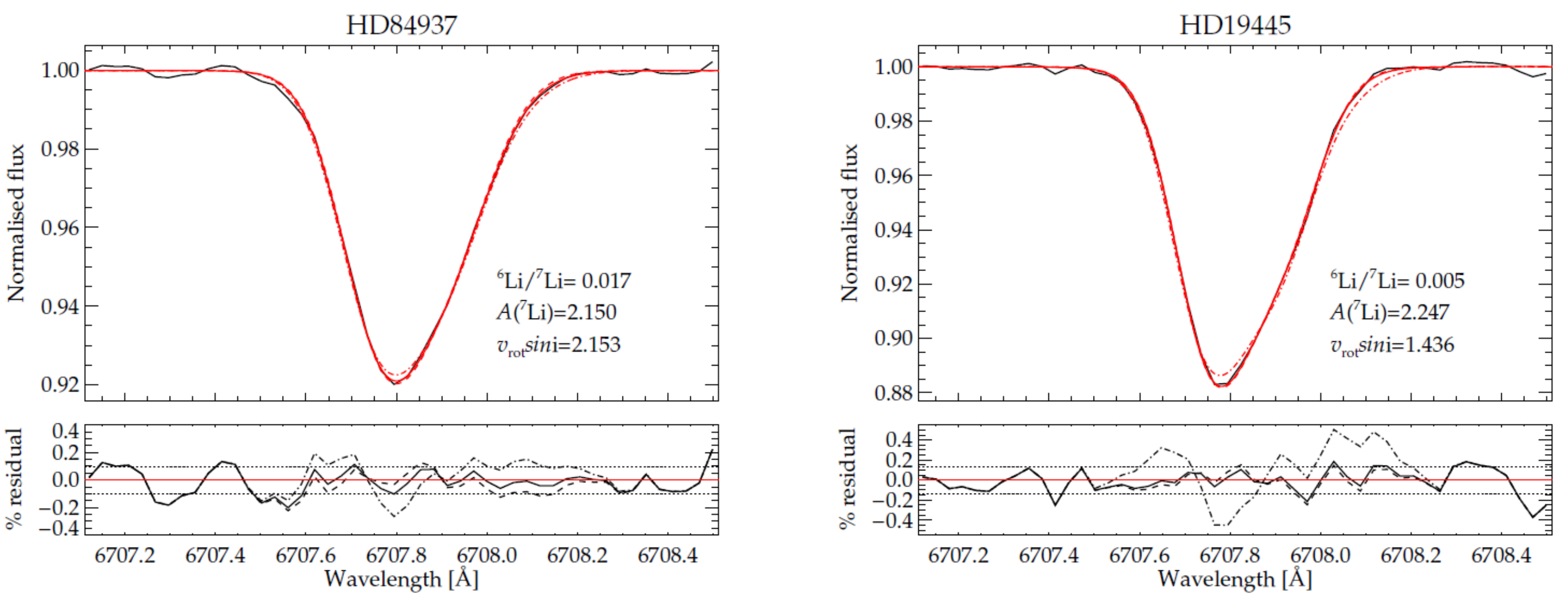

Fig. 8. Observed line profiles (black solid lines) and best-fit 3D, NLTE synthetic profiles. The projected rotational velocity has been constrained by calibration lines. Below each panel the flux residual (observed-synthetic) in per cent is shown. The three line profiles correspond to the best-fit value indicated in the plot (solid line), ^{6}Li/^{7}Li = 0.0 (dashed line) and ^{6}Li/^{7}Li = 0.05 (dotted-dashed lines). The estimated observational uncertainty per pixel is also indicated (dotted horisontal lines).

Measurement of isotopes: molecular lines

Large effect of mass difference on molecular spectra

CH molecules

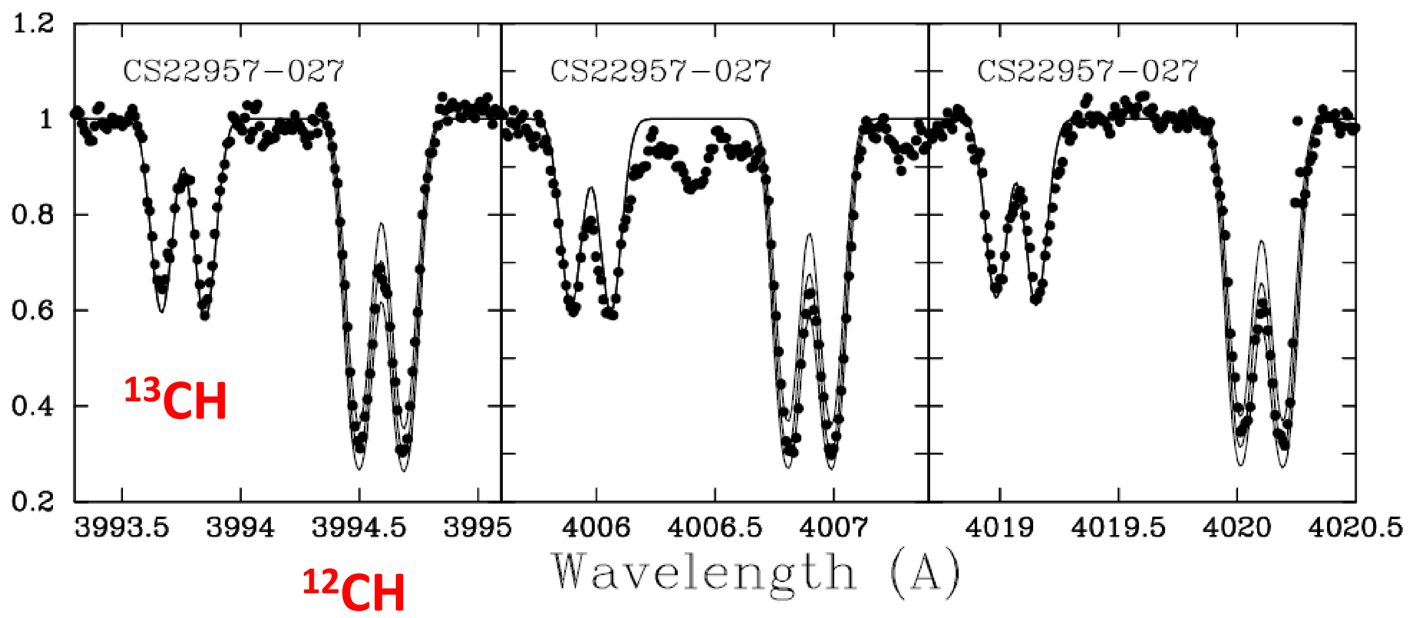

Aoki et al. (2002)

Mg isotopes

MgH molecular lines

$^{24}Mg/^{25}Mg/^{26}Mg$

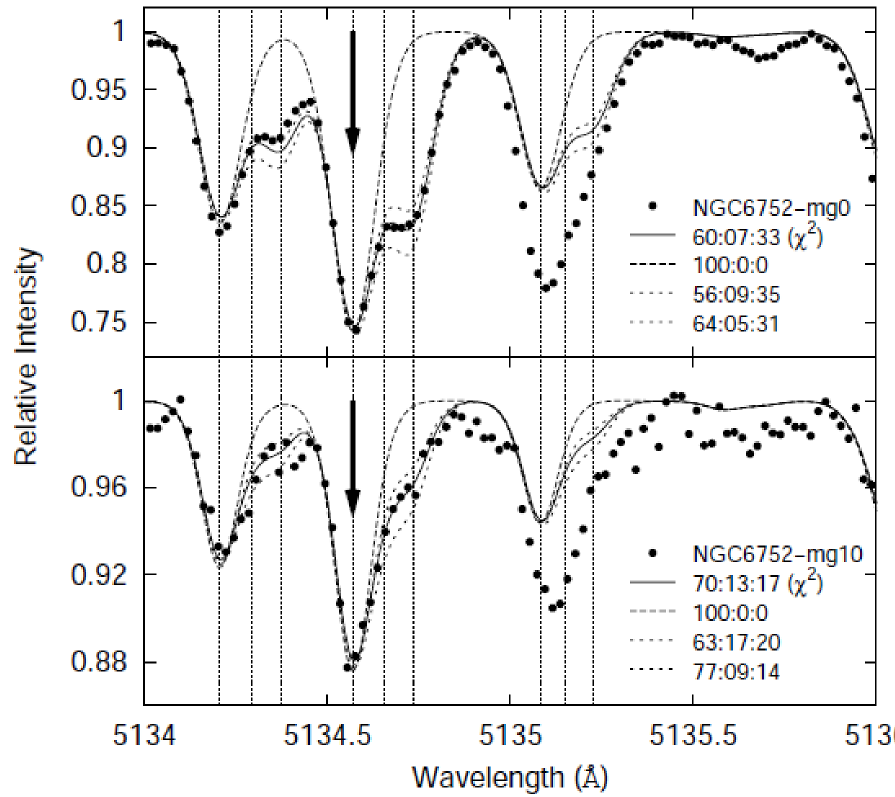

Fig. 7. Spectra of NGC 6752-mg0 (upper) and NGC 6752-mg10 (lower) from 5134.0 to 5136.0 Å. The feature we are interested in fitting is highlighted by the arrow. The positions of the ^{24}MgH, ^{25}MgH, and ^{26}MgH lines are indicated by dashed lines. The closed circles represent the observed spectra. The synthetic spectrum generated using the isotopic ratios determined by χ^2 analysis is given by the solid line: the ^{24}Mg:^{25}Mg:^{26}Mg ratios are given on the figure. Unsatisfactory ratios are plotted as dotted lines.

Yong et al. (2003)

Measurement of isotopes: hyperfine splitting of spectral lines of heavy elements

Large effect of hyper fine splitting on spectral lines of heavy elements that depends on isotopes

- **Splitting of spectral lines due to difference of nuclear spin**

- **Large effect on odd nuclei**

Ba isotopes

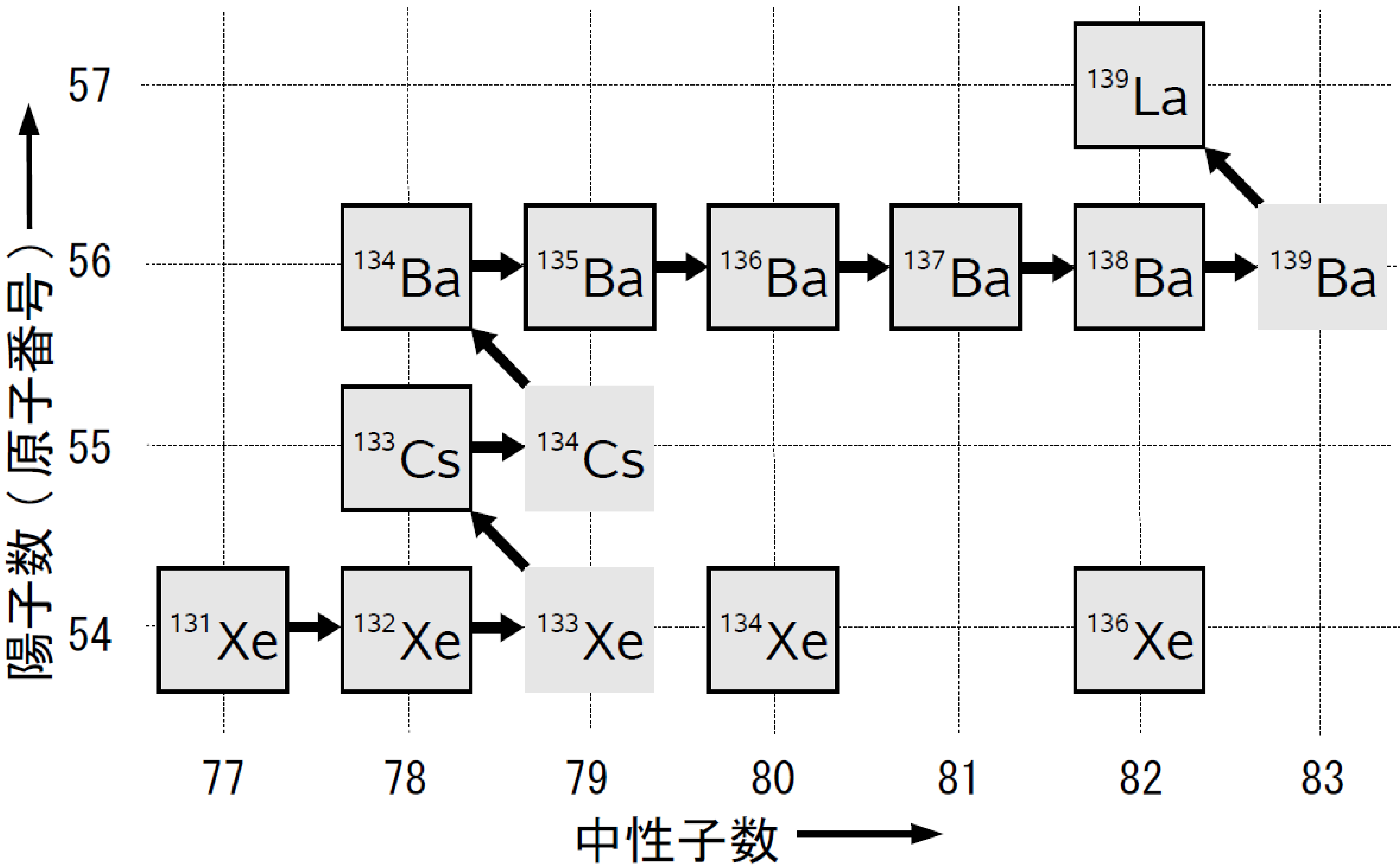

57
56
55
54
陽子数（原子番号）
139La
134Ba
135Ba
136Ba
137Ba
138Ba
139Ba
133Cs
134Cs
131Xe
132Xe
133Xe
134Xe
136Xe
77
78
79
80
81
82
83
中性子数

Measurement of Ba isotope ratios

Ratio of isotopes with odd (135, 137) and even (134, 136, 138) mass number is measurable

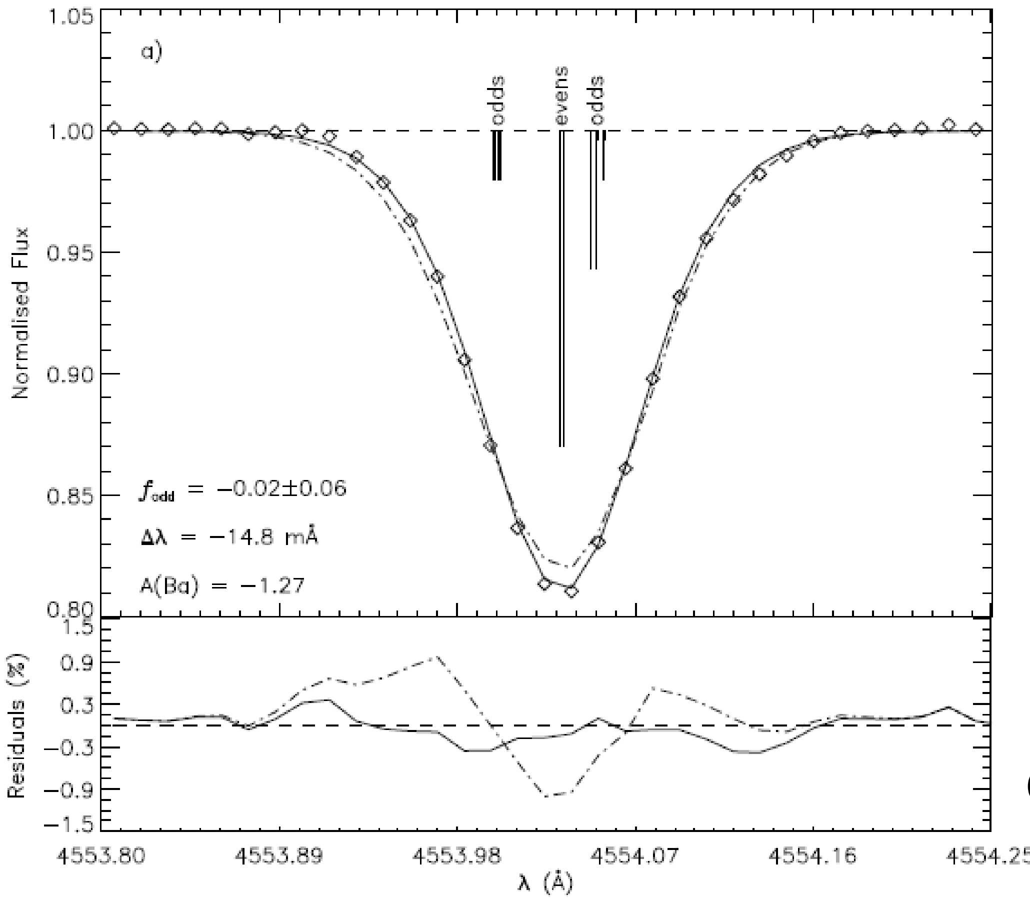

Gallagher et al. (2010)

Eu isotopes

Eu: atomic number=63, mass number=151 or 153

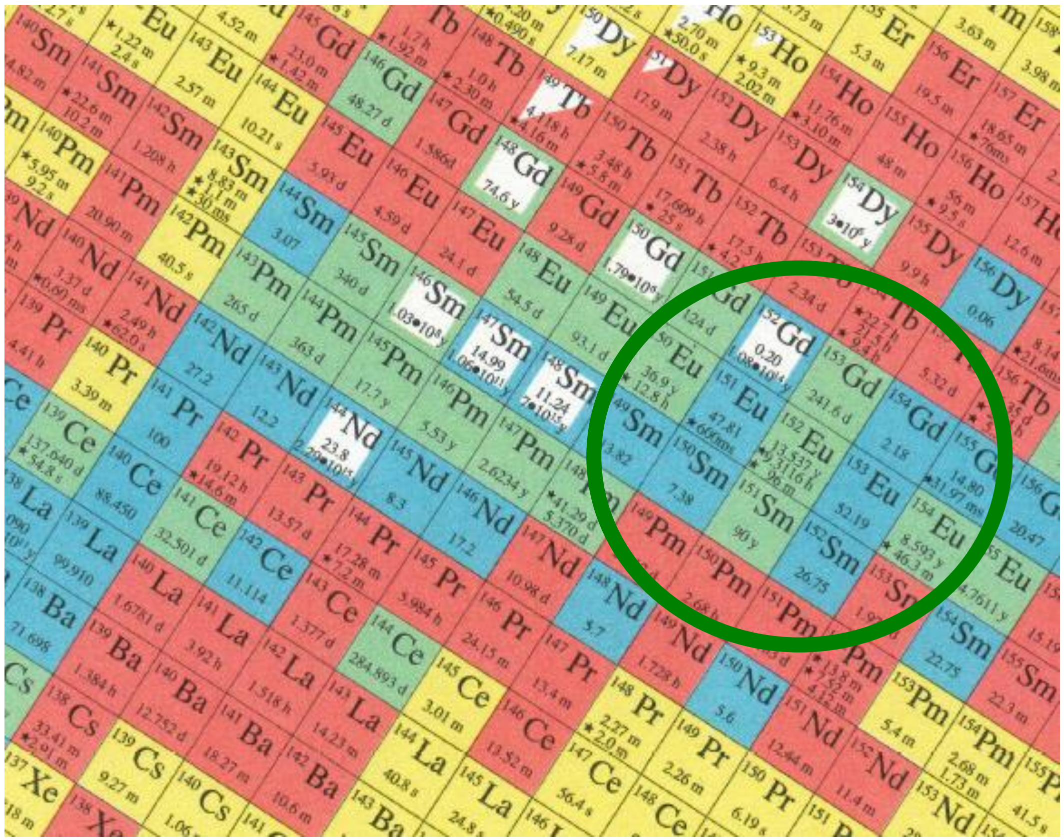

Eu isotopes ～ easiest case?

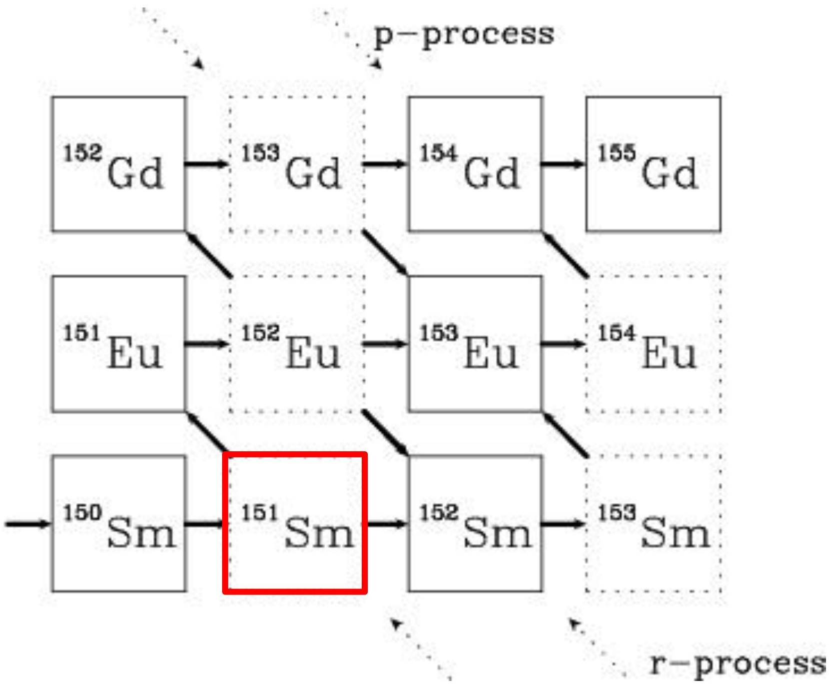

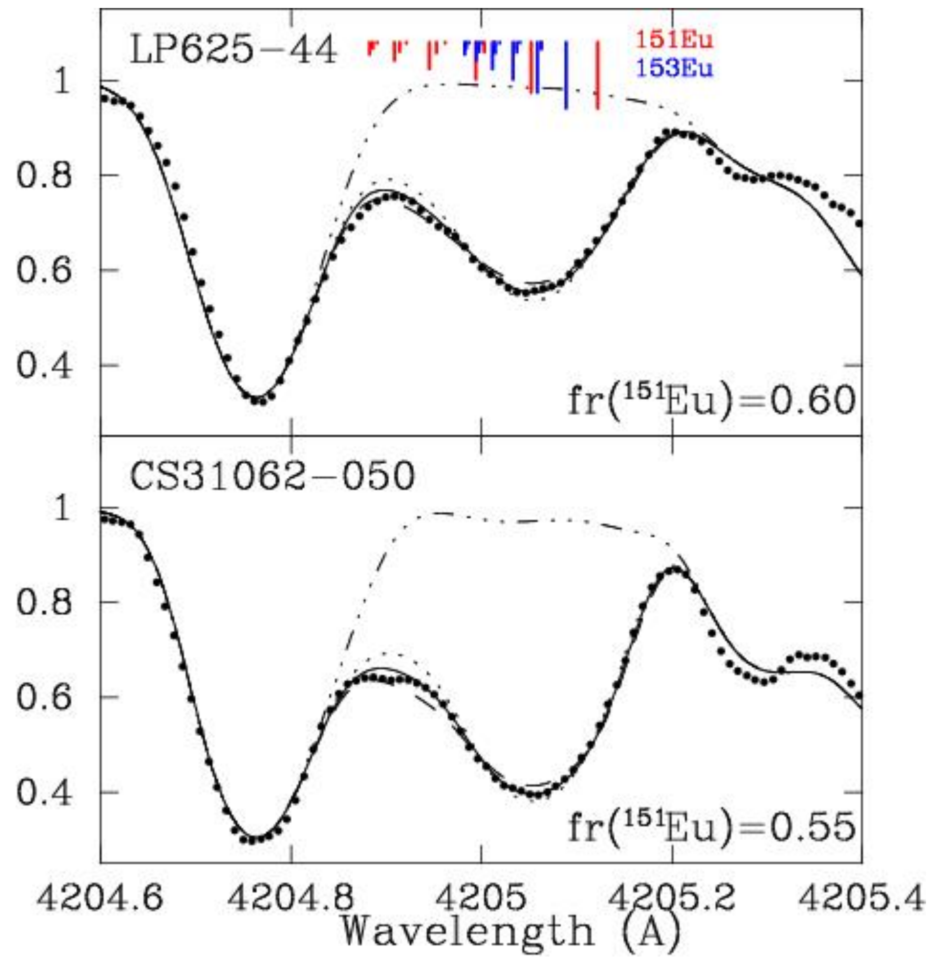

Aoki et al. (2003)

Lithium as a tracer of chemical evolution

Lithium

A variety of origins

→A useful element to examine nucleosynthesis in the cosmos

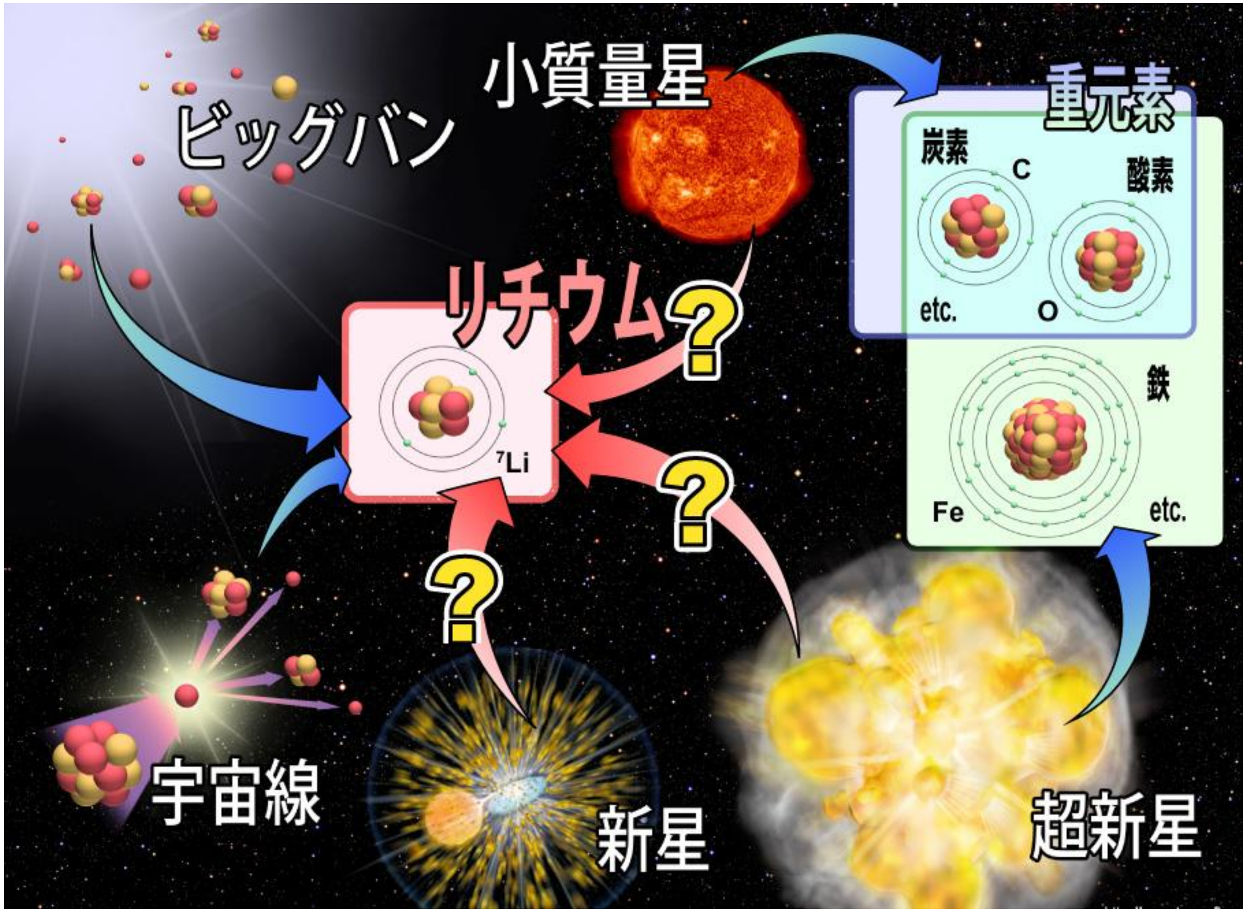

However, direct observational evidence of Li production events is sparse.

Li isotopes in the solar-system

- **Meteorite:**
  $\log \varepsilon(\mathrm{Li}) = \log(N_{\mathrm{Li}}/N_{\mathrm{H}})+12$
  $= 3.26$
  $^{7}\mathrm{Li}/^{6}\mathrm{Li}=12.5$
- **Photosphere:**
  $\log \varepsilon(\mathrm{Li}) = 1.05$

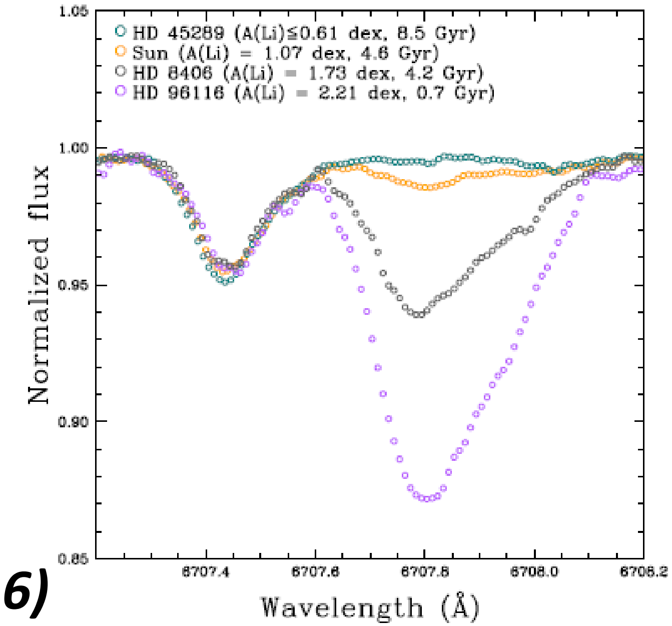

Carlos et al. (2016)

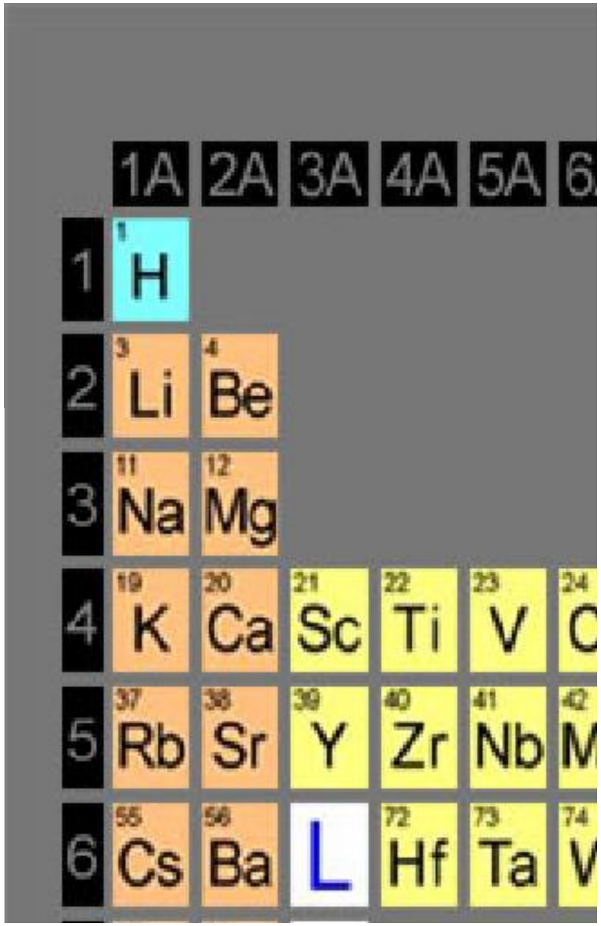

1. Li production in Big-Bang nucleosynthesis

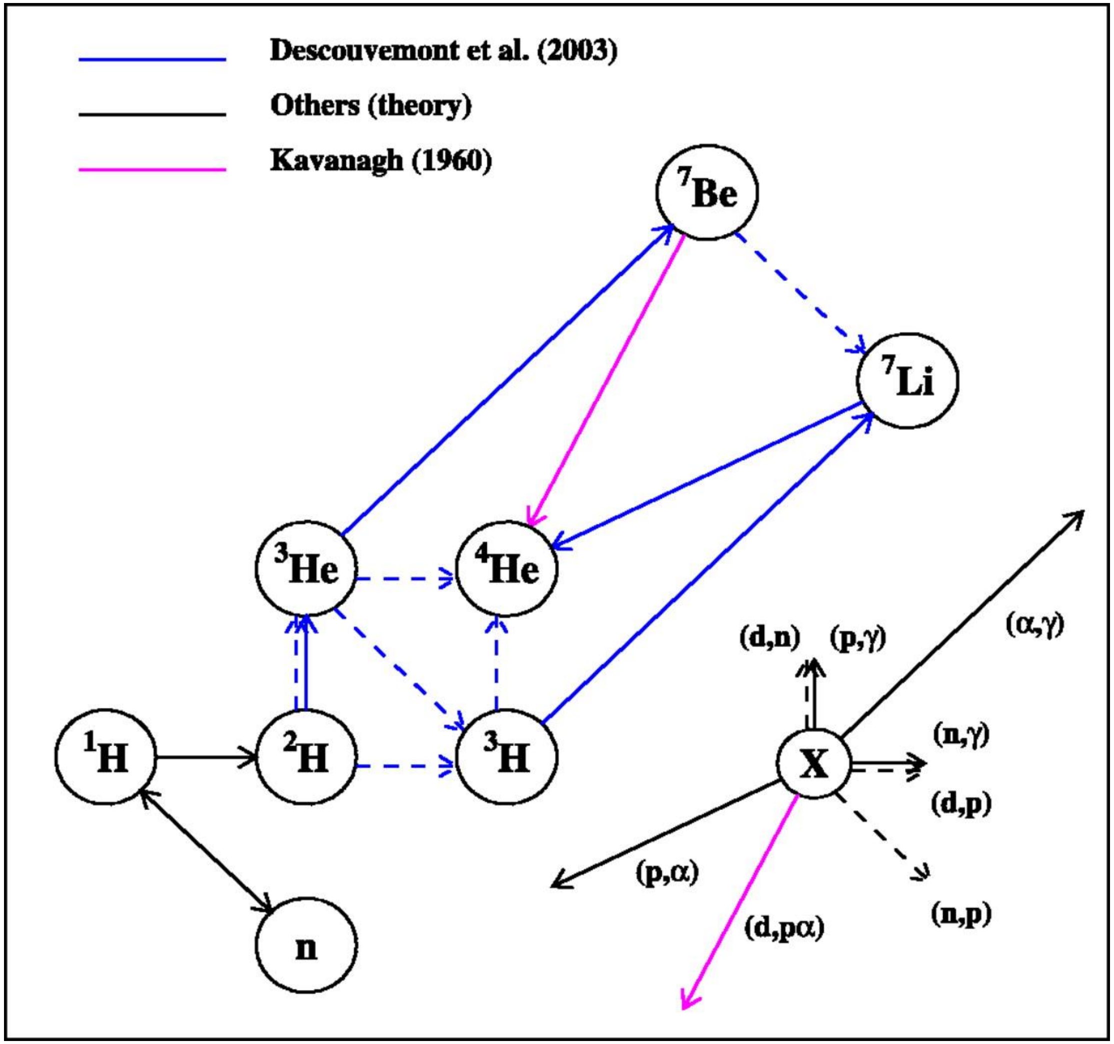

Coc et al. (2004)

Big-Bang nucleosynthesis

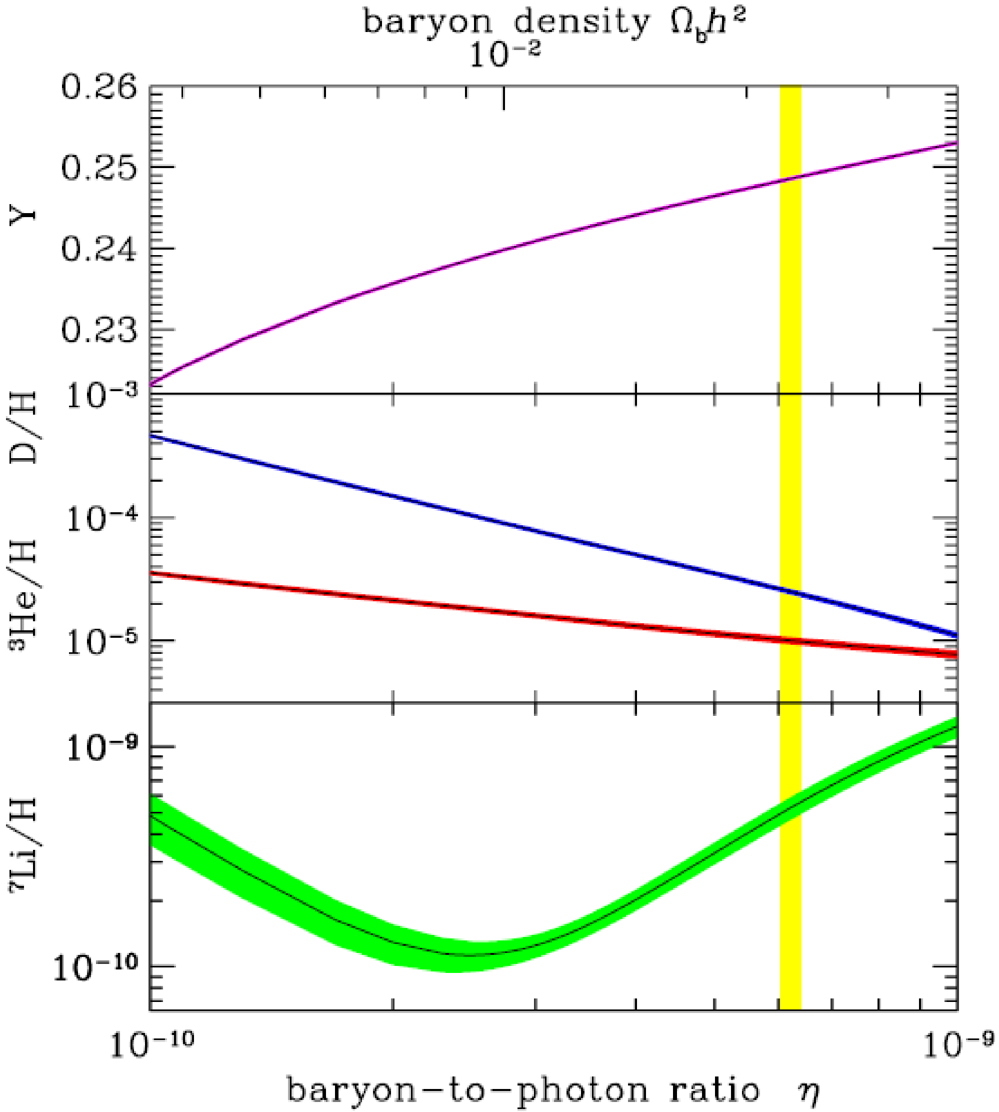

Cyburt et al. (2008)
cf. review by Cyburt et al. (2015)

2. Li production by Cosmic-ray (CR) spallation

- CR (CNO) + ISM(pα)
  ‘primary’

- ISM(CNO) + CR(pα)
  ‘secondary’

- $\alpha + \alpha \rightarrow {}^{6}Li$

  ${}^{7}Li/{}^{6}Li \sim 2$

Prantzos (2012)

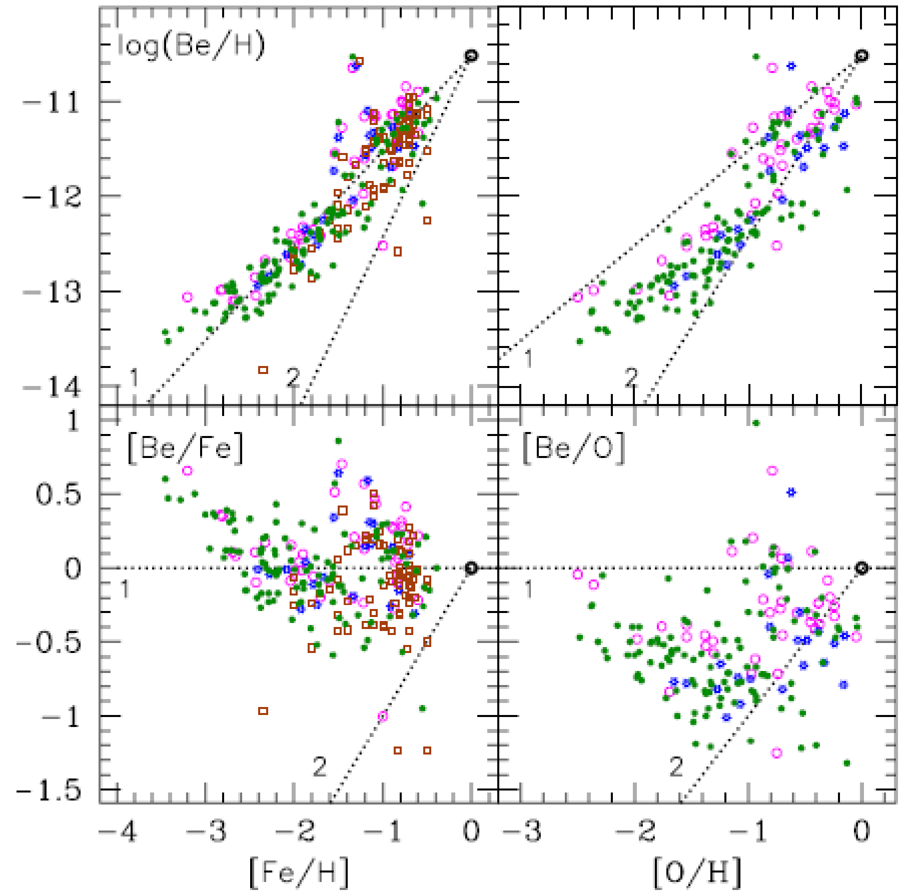

Fig. 1. Observations of Be vs. Fe (*left*) and vs. O (*right*). In all panels, dotted lines indicate slopes of 1 (primary) and 2 (secondary). Data are from Primas (2010, circles), Tan et al. (2009, asterisks), Smiljanic et al. (2009, open squares), and Boesgaard et al. (2011, dots).

3. Li production in low-mass stars

'beryllium transport (Cameron-Fowler) mechanism'

- **He shell:**
  $^3He+\alpha \rightarrow {}^7Be$

- **Stellar surface:**
  $^7Be + e \rightarrow {}^7Li$

(half-life of ^7Be is 53 days)

Abia et al. (1999)

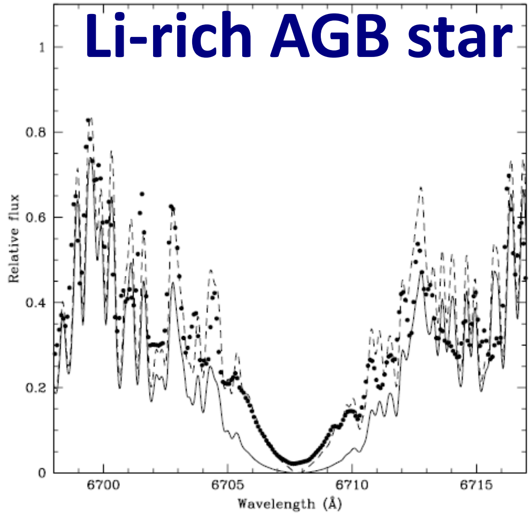

Fig. 5. As Fig. 4 in the λ6708 Å spectral domain of WZ Cas for log ϵ(Li)=5.0

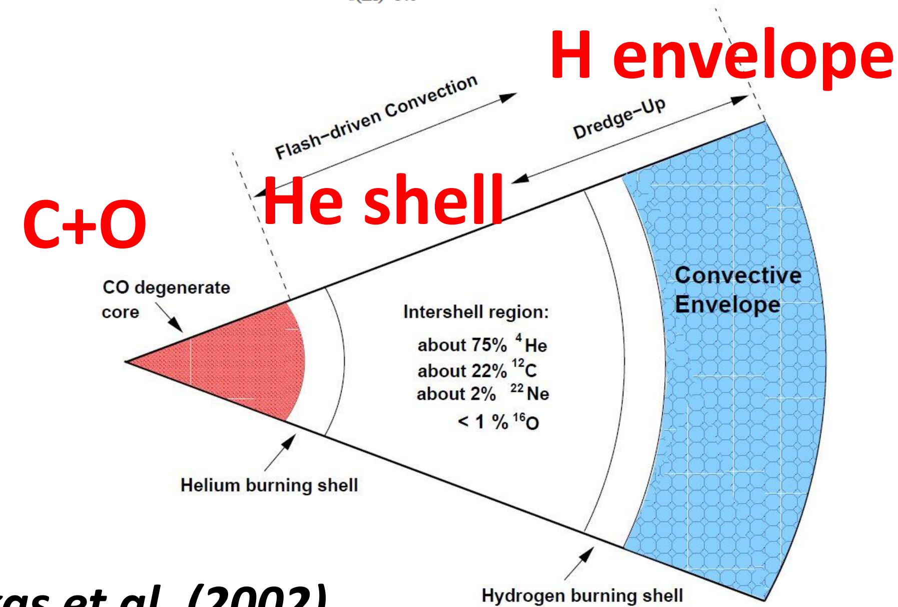

Karakas et al. (2002)

Li-rich giant (AGB) stars in Magellanic clouds

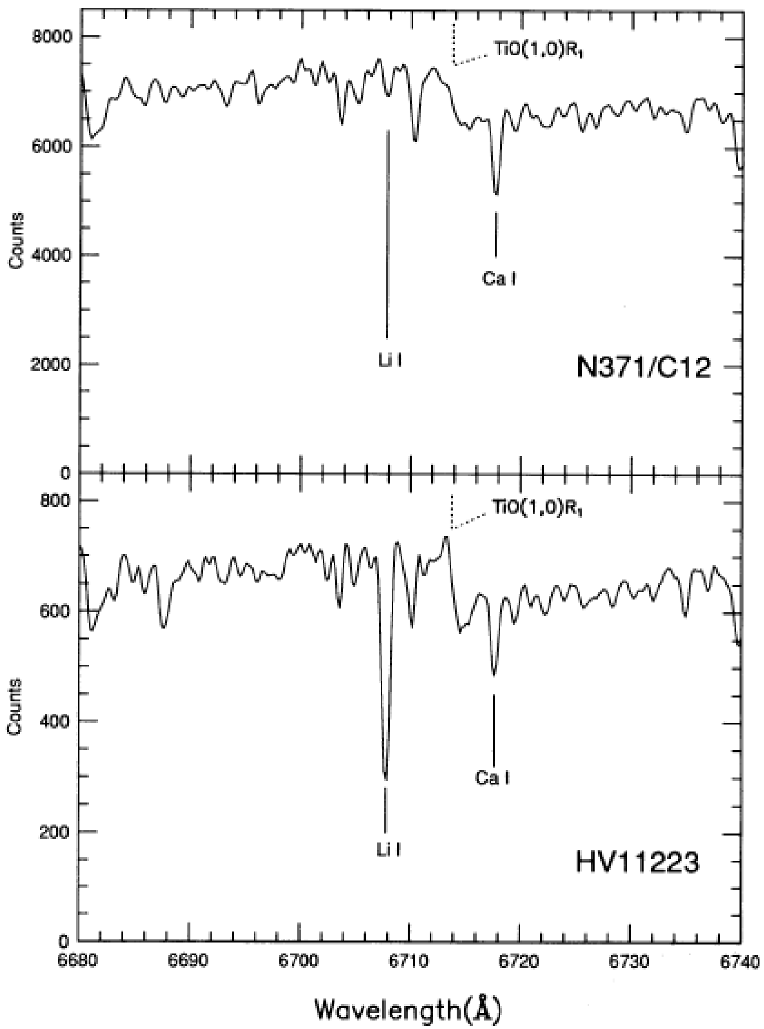

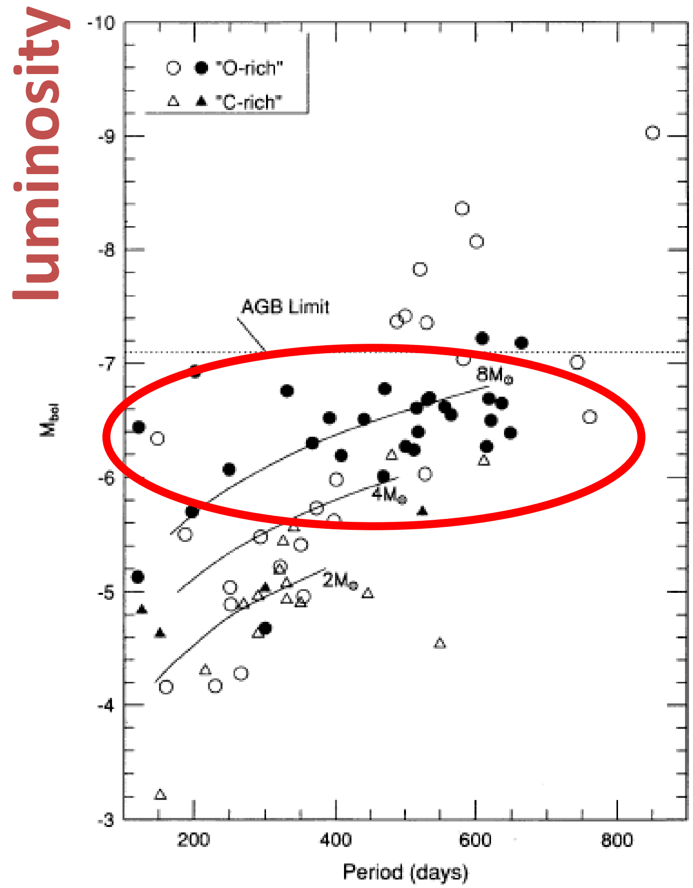

FIG. 6.—Combined M_{bol}-P diagram for the Magellanic Clouds with the filled symbols denoting the Li-strong stars. The segregation of the Li-strong stars to the most luminous of the AGB stars is striking. Note that no AGB stars with detectable Li I are found at luminosities significantly exceeding the AGB limit. A few AGB stars with $M_{bol} > -6$ show detectable Li I lines. The solid curves denote evolutionary tracks for AGB stars taken from the equations given in Wood et al. (1983) for fundamental pulsators.

Plez et al. (1993) ***Smith et al. (1995)***

4. Li production in novae

e.g. Boffin et al. (1993)

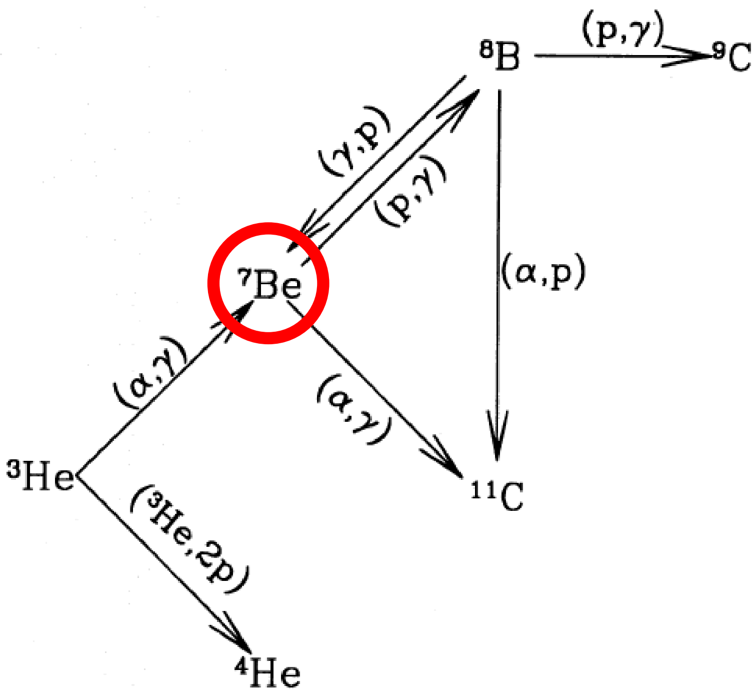

Fig. 1. Main nuclear reactions involved in the synthesis of ^{7}Be for typical explosive hydrogen burning conditions. The post-freeze-out ^{7}Be($e^-\nu$)^{7}Li transformation is not indicated

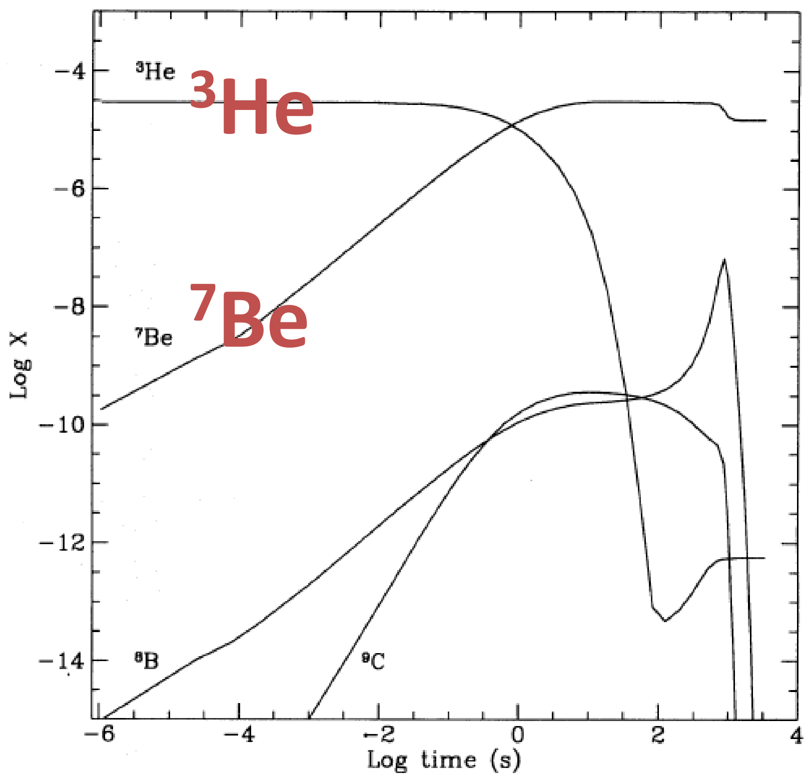

Fig. 4. Time evolution of the mass fractions of ^{3}He, ^{7}Be, ^{8}B, and ^{9}C for the case T_0 = 3 10^8 K, ρ = 100 gcm^{-3}, and τ_{ex} = 300 s

5. Li production in Supernovae -- ν-process

ex. $^4He(\nu,\nu' p)^3H(\alpha,\gamma)\,^7Li$

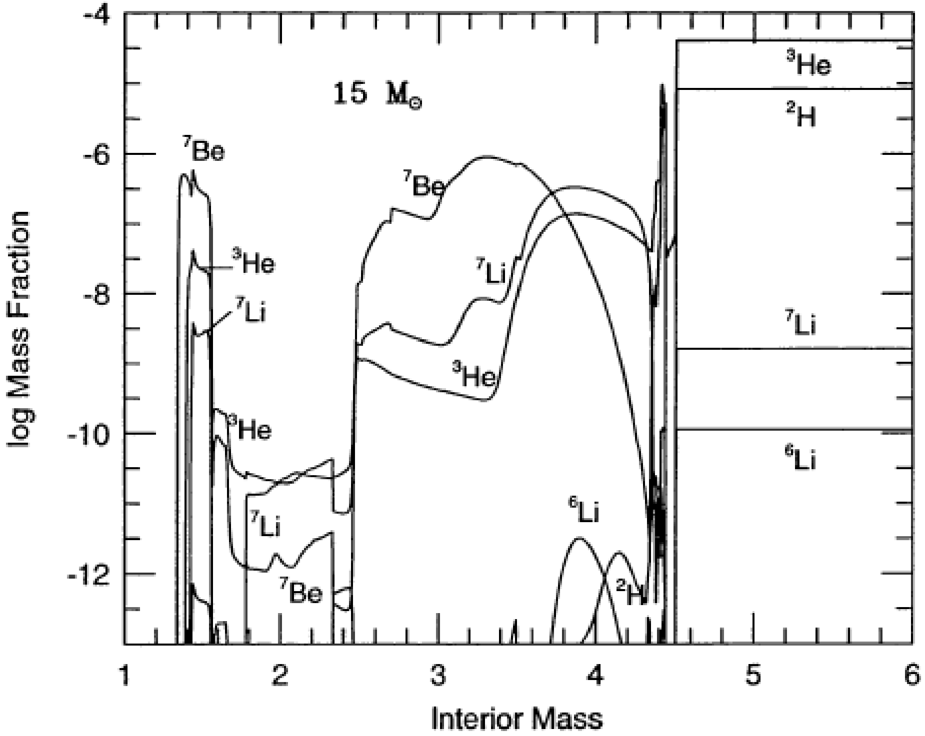

Woosley & Weaver (1995)

Li abundances in stellar atmospheres

- Destruction of lithium

  ^{7}Li destruction with *T>2.5* Million K

  $^7Li + p \rightarrow {}^4He + {}^4He$

  ^{6}Li destruction with *T>2* Million K

  $^6Li + D \rightarrow {}^4He + {}^4He$

  $^6Li + p \rightarrow {}^4He + {}^3He$

- Li is depleted at the surface of stars in which convective envelope is sufficiently thick.

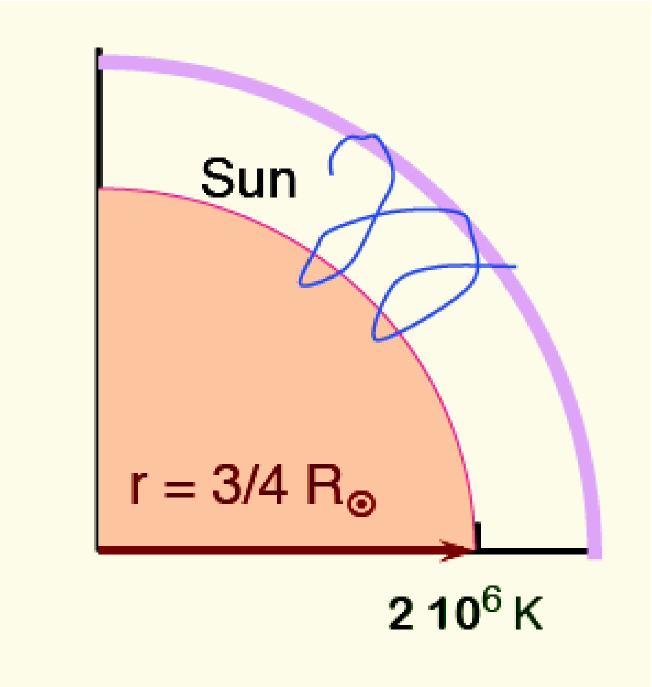

Spite (Li in the Cosmos)

Lithium in main-sequence stars in clusters

Pleiades: a young cluster (80Myr)

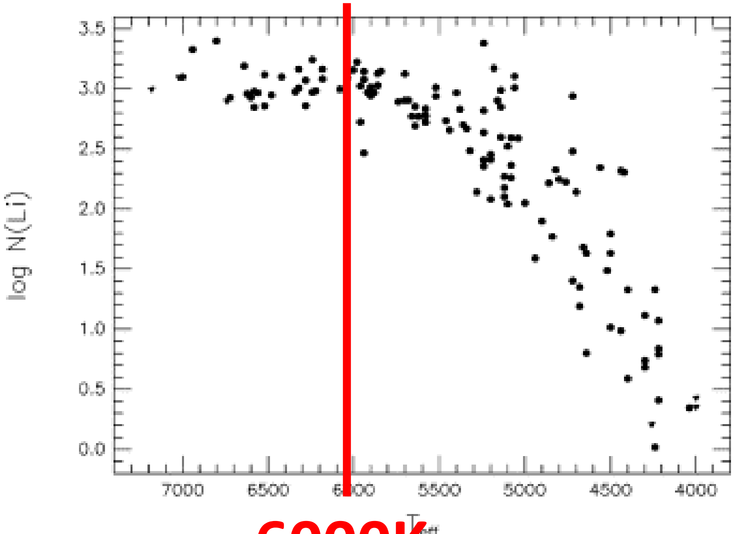

Hyades: an"old" cluster (600Myr)

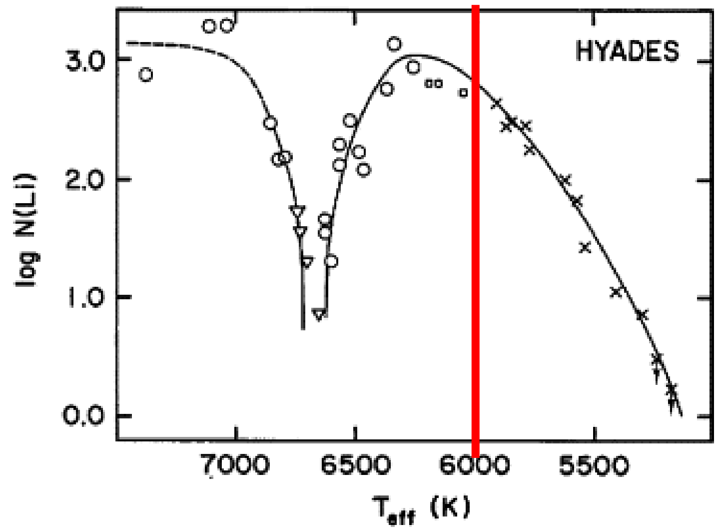

6000K

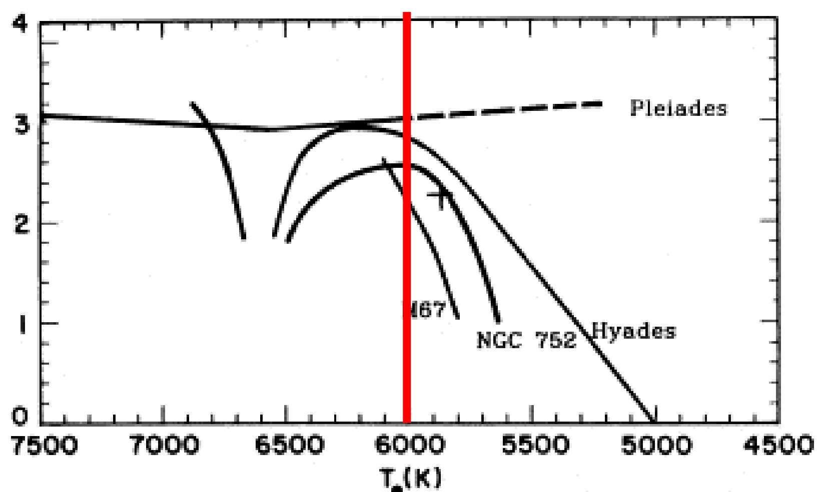

Effective temperature

Hobbs (2000)

Lithium in metal-poor stars

Shallow convective layer in metal-poor stars →small depletion of lithium

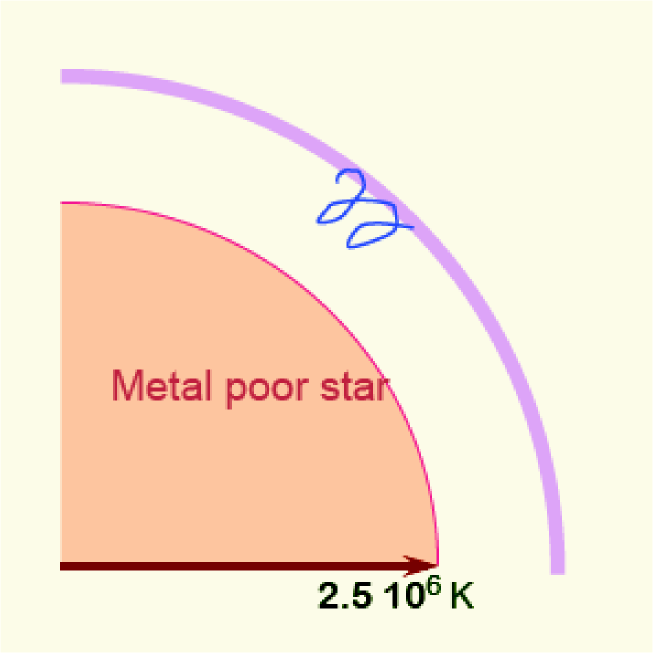

Spite (Li in the Cosmos)

Metal-poor stars near the main-sequence turn-off with shallow convective envelop

Turn-off stars for which Li is measured

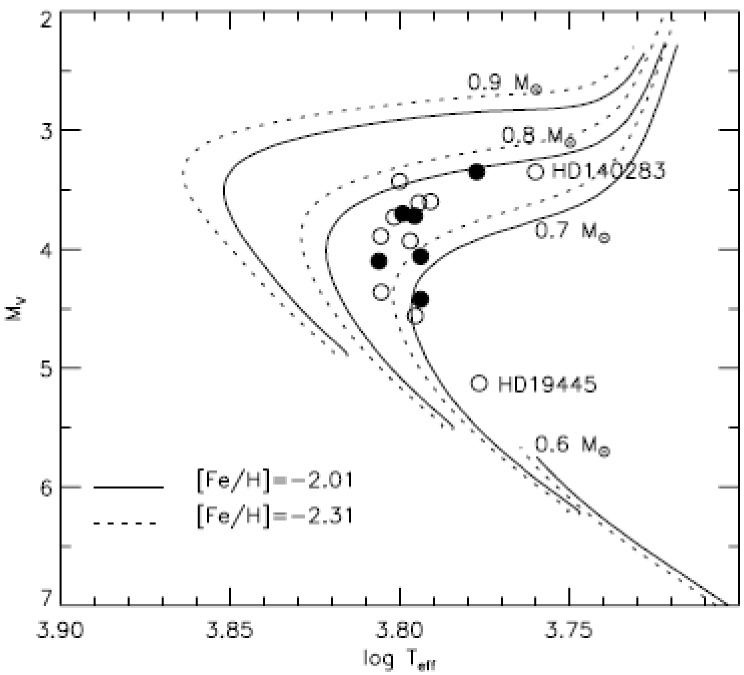

Asplund et al. (2006)

HR diagram of globular cluster stars

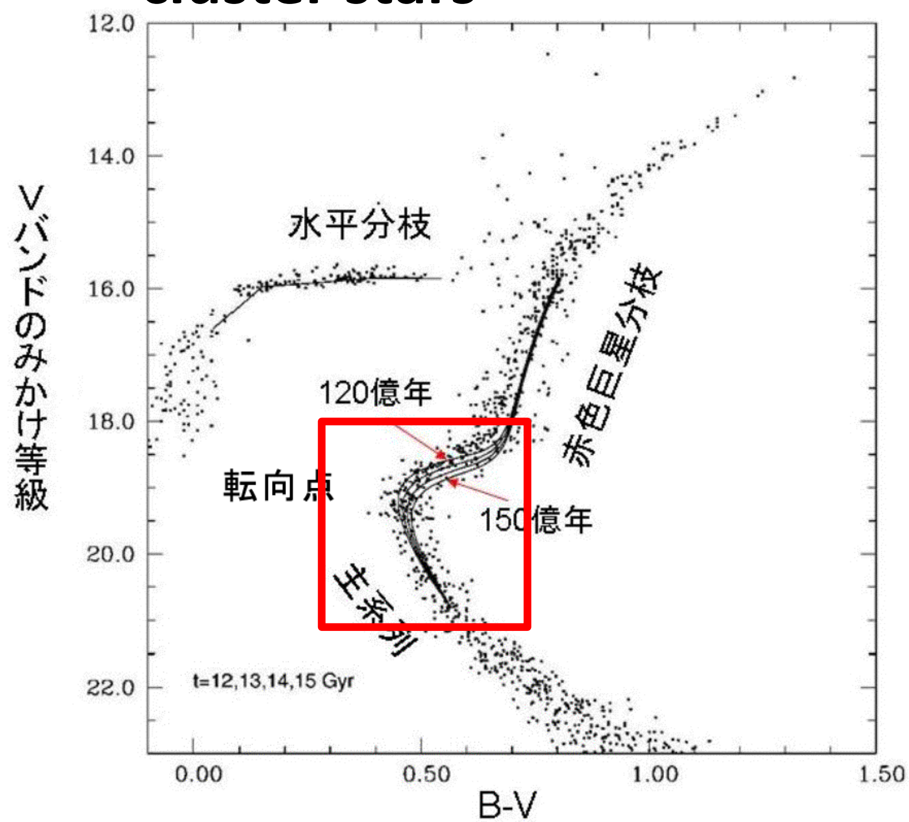

"Spite Plateau"

Constant Li abundances in metal-poor stars, in which convective envelope is thin.

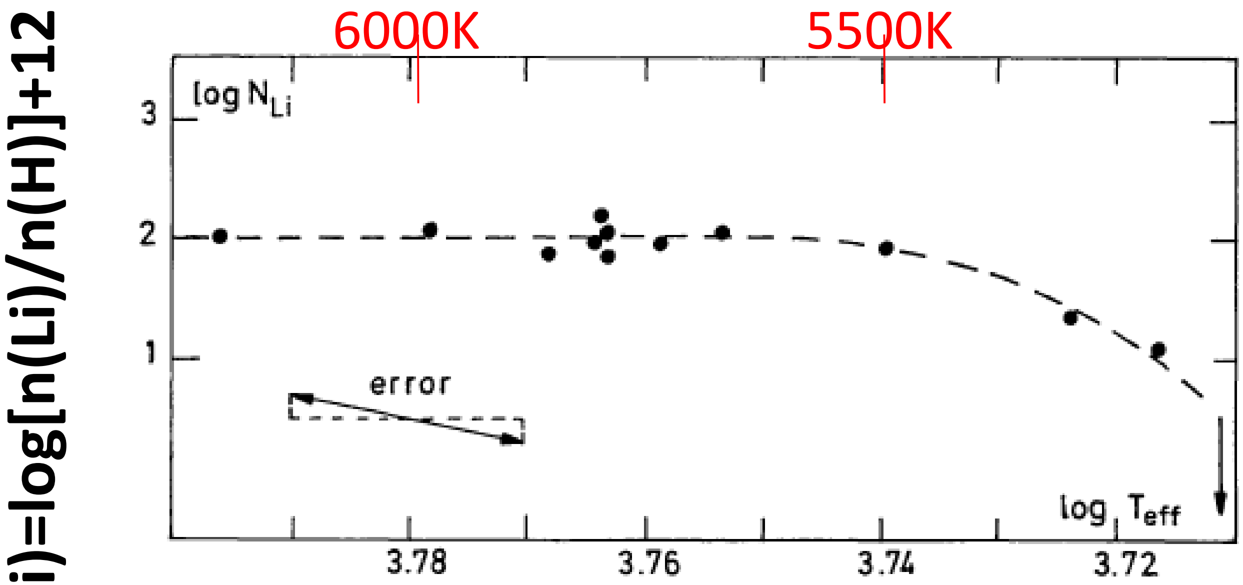

Fig. 5. N_{Li} versus $\log T_{\mathrm{eff}}$ for old halo stars

Spite & Spite (1982)

Spite Plateau and Li evolution in the Galaxy

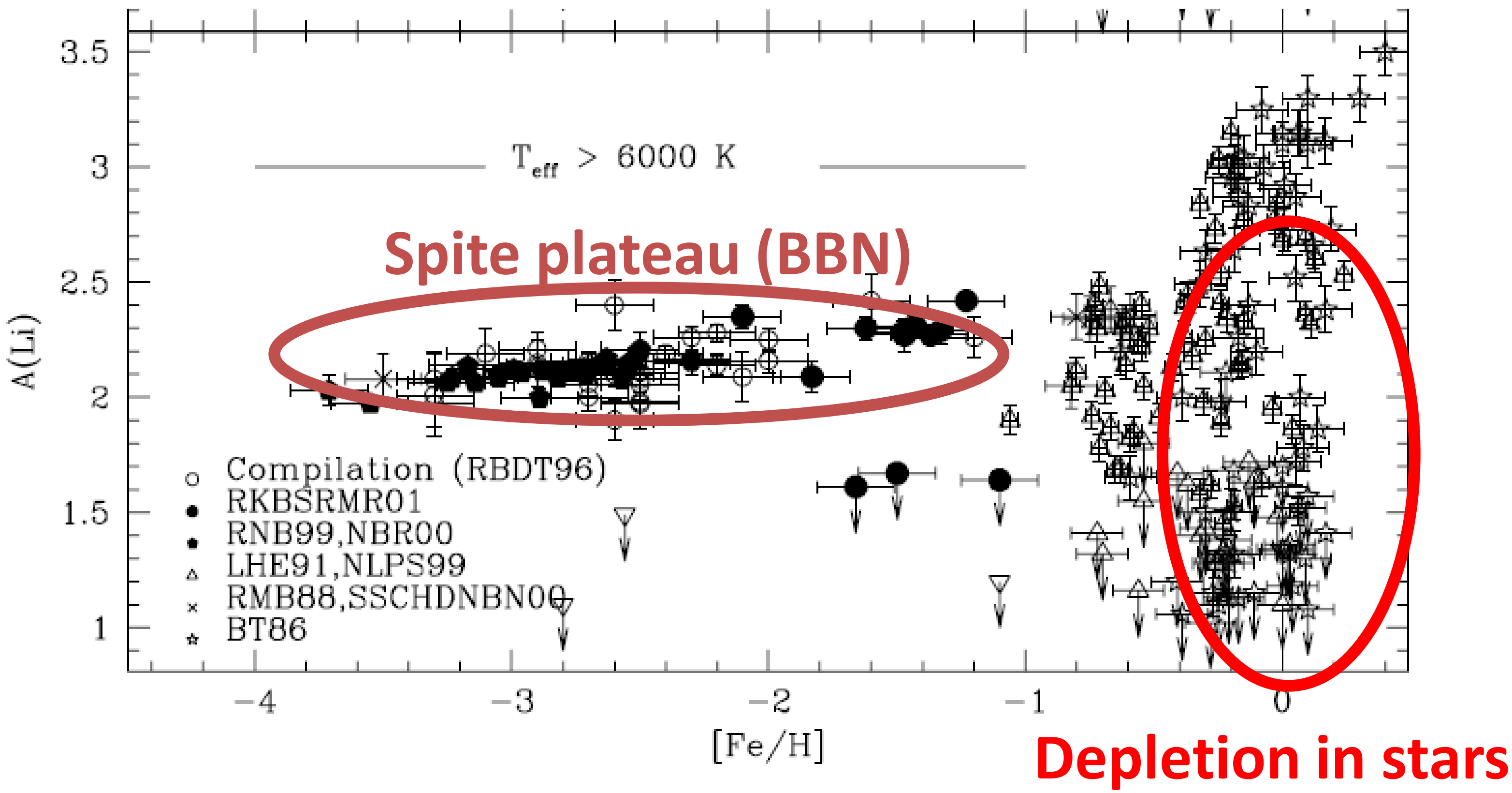

Ryan et al. (1999)

Modeling of the evolution of Li in the Galaxy

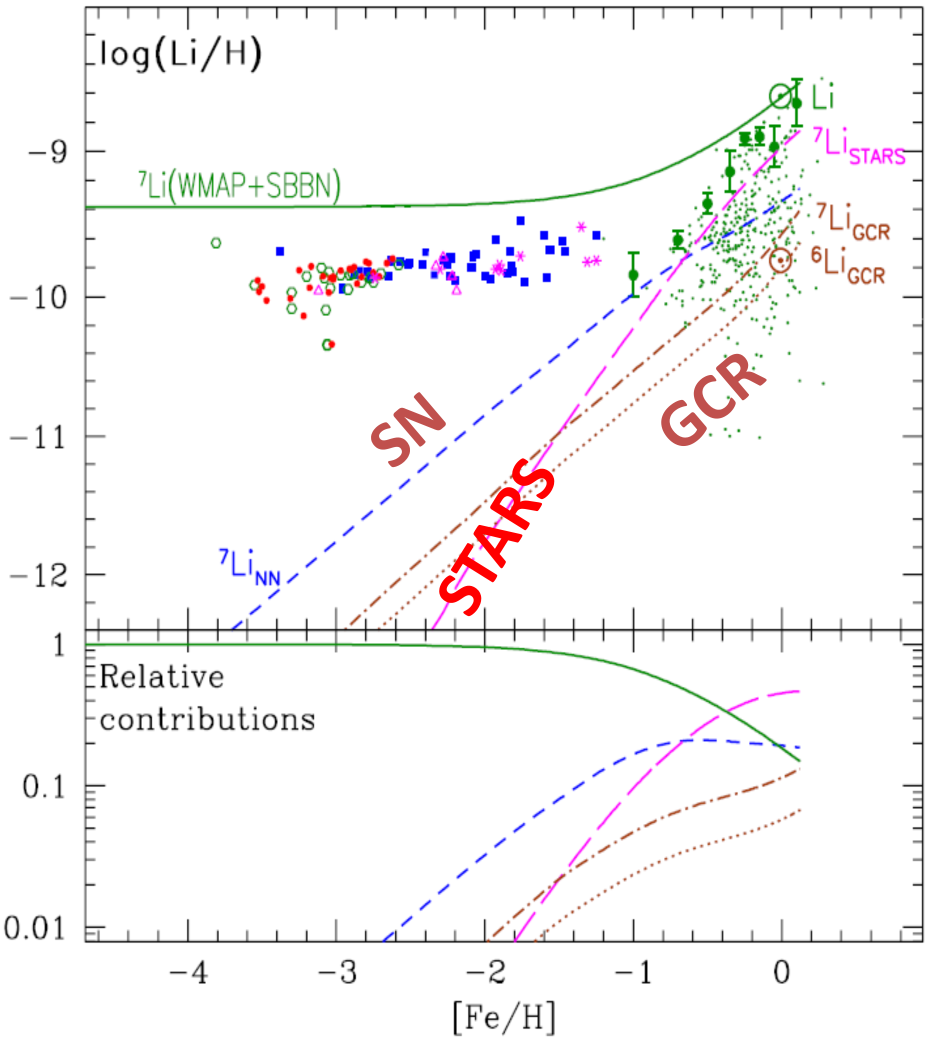

- **Low-mass stars: 'STARS' including novae**
- **Cosmic rays: 'GCR'**
- **Supernovae: 'SN'**

Prantzos (2012)

Classical novae

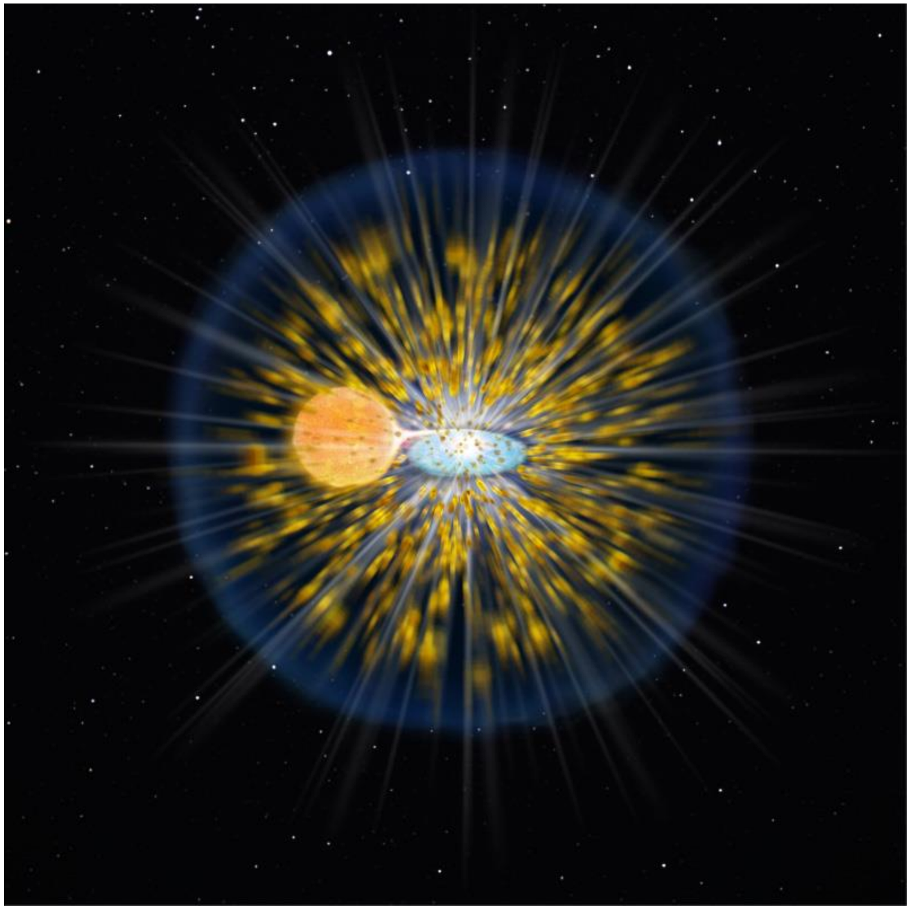

5-10 events per year observed in the Milky Way

- Binary system with a white dwarf and a main-sequence star or a red giant
- Mass accretion from a companion to white dwarf forming accretion disk

Igniting nuclear fusion when the gas layer become sufficiently hot and dense
→explosive reaction ejecting the gas layer

High velocity absorption lines in nova spectra

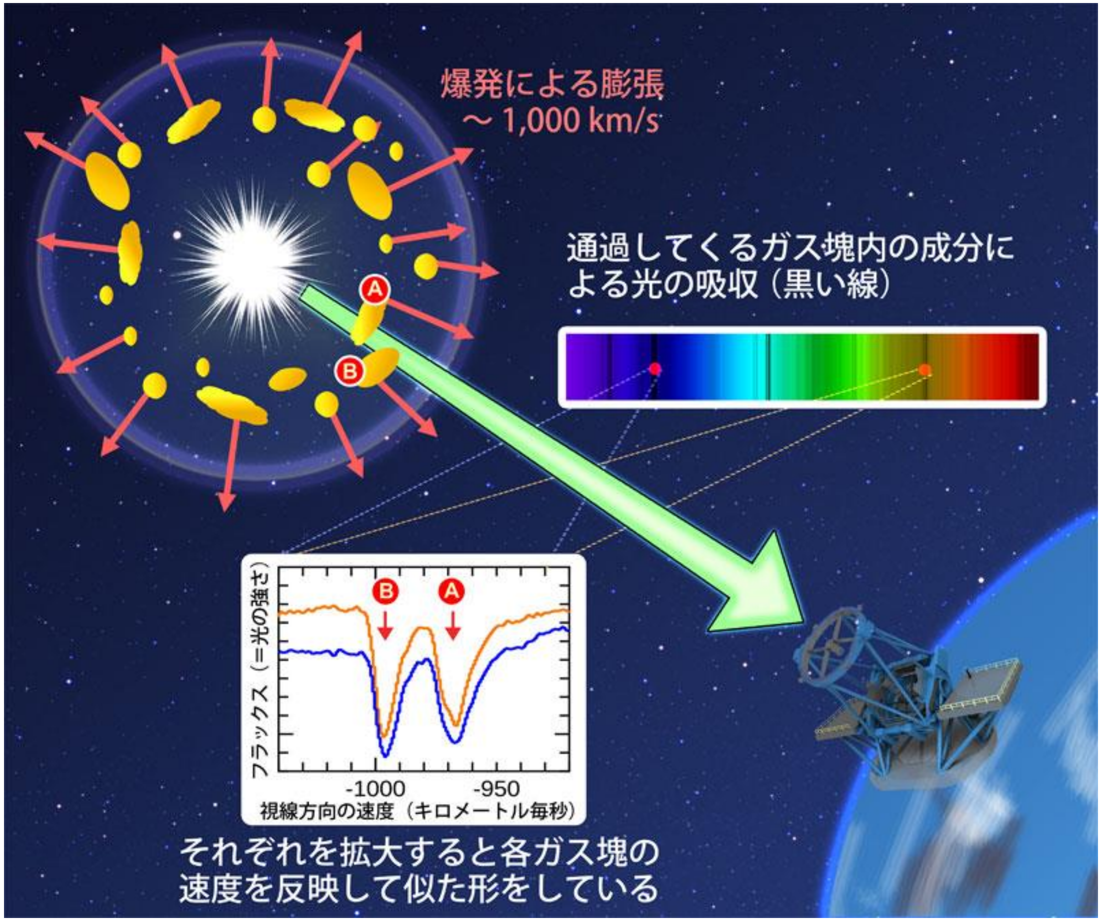

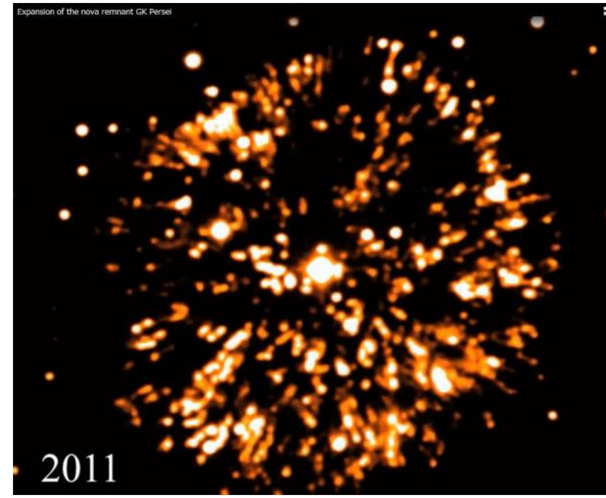

Liimets et al., (2012)

Nova 1901 Per (GK Per)

110 years after the explosion

Absorption by gas clumps ejected from the white dwarf surface by explosion

Discovery of ^{7}Be in a nova spectrum

Tajitsu et al.(2015, Nature 518, 381)

- 47 days after the explosion
- Two high velocity absorption components at
  -1,103 km/s
  -1,268 km/s

Detection of doublet ^{7}Be absorption line at 312nm (UV region)

Velocity is adjusted by one of the ^{7}Be II doublet lines (shown by red: A and C), which agrees the velocity estimated for H and Ca lines

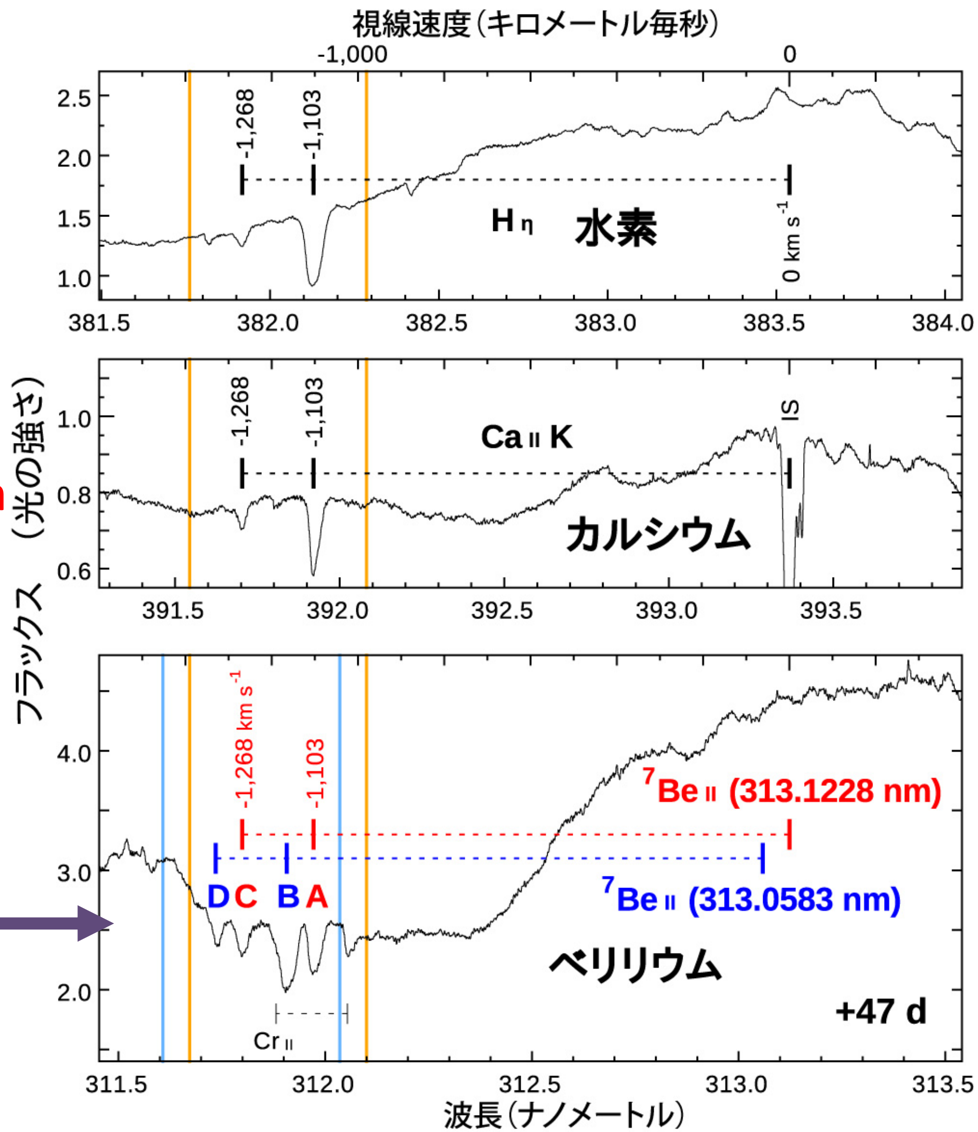

^{7}Li production in classical novae

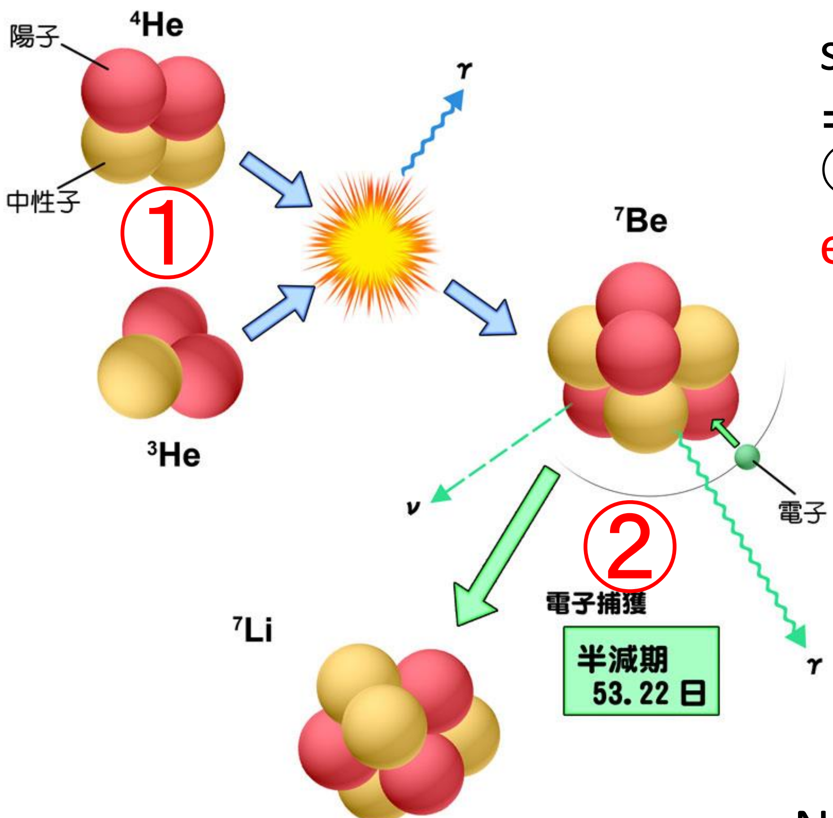

①hydrogen burning at the surface of a white dwarf

⇒ $^3He(\alpha,\gamma)^7Be$ reaction

②electron capture forming ^{7}Li in ejected gas

Short half life of 7Be (53.2 days) indicates that it is synthesized in the object very recently.

No observational evidence until 2015.
γ-ray emission at 478keV by electron capture has not yet been detected.

Another evidence: Li absorption line in classical nova spectra

Nova 1369 Cen

Absorption line of neutral Li in spectra of earlier phase of (different) nova

Novae are certain site of Li production

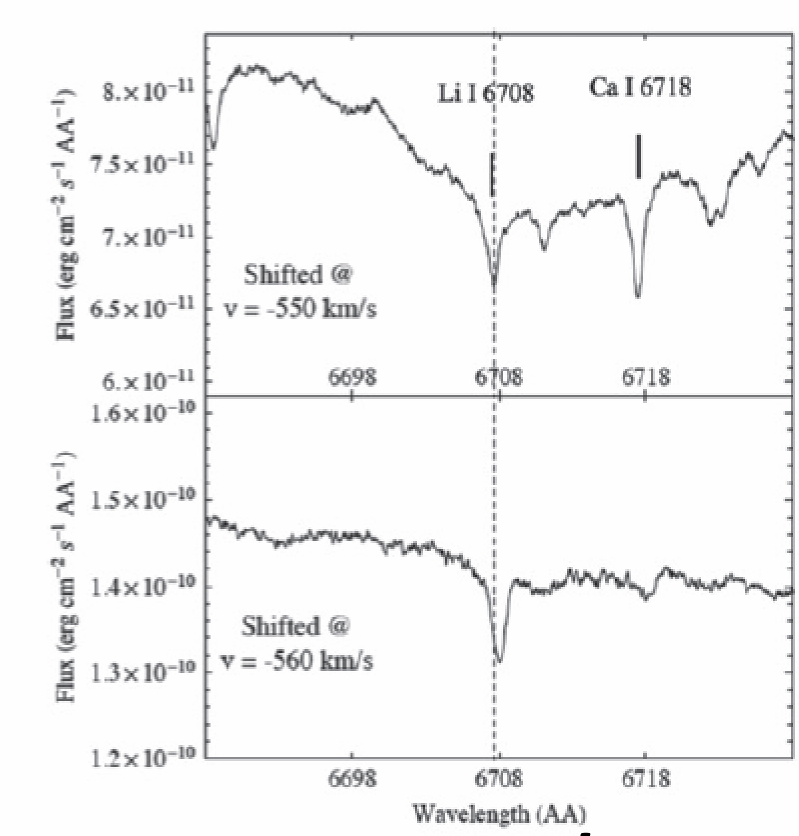

7 days

13 days

Izzo et al. (2015)

Li isotope ratios in interstellar matter and supernova remnant

- Big-bang, supernovae(ν-process), low-mass stars → ^{7}Li
- Cosmic-ray spallation→$^{7}Li/^{6}Li$ ~ 2
- Solar-system material
  $^{7}Li/^{6}Li=12.5$
- Nearby clouds
  $^{7}Li/^{6}Li$～8

Inhomogeneous Li isotope ratios in ISM?

Solar-system material
$^{7}Li/^{6}Li=12.5$

- **Nearby clouds**
  $^{7}Li/^{6}Li \sim 8$

- **ρ Oph**
  $^{7}Li/^{6}Li=12.5$
  Lemoine et al. (1993)

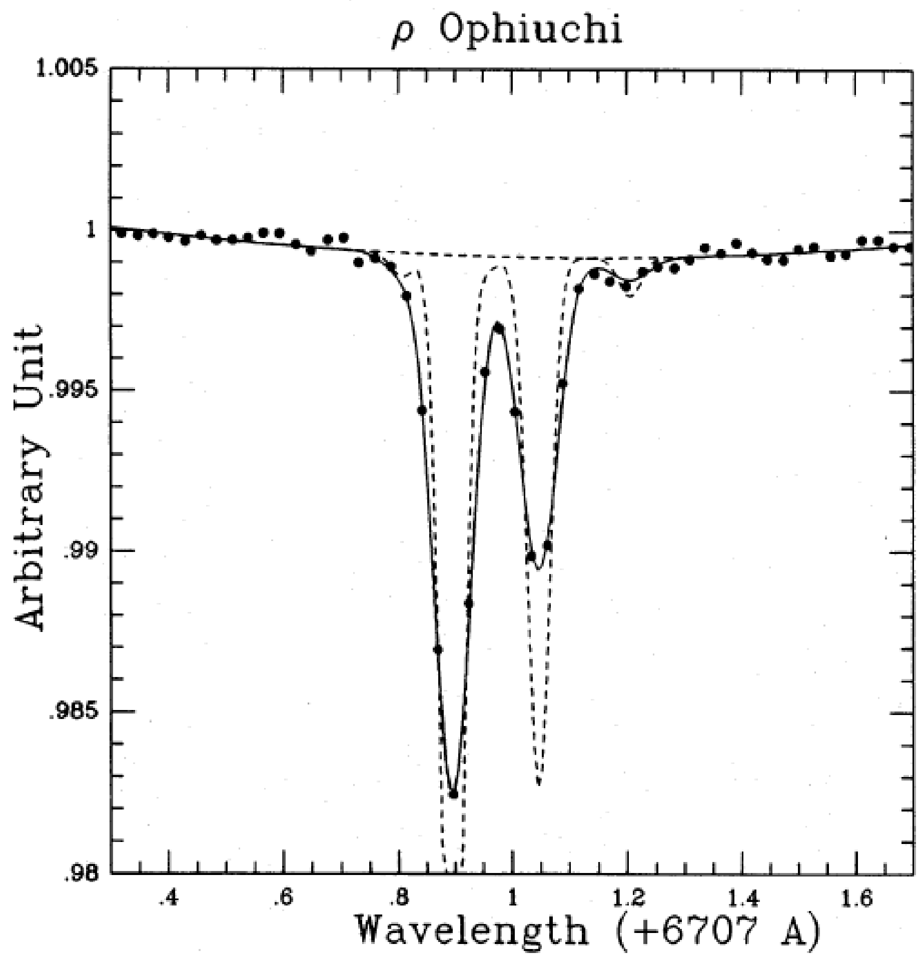

Fig. 7. Final fit of the Li lines assuming two clouds on the line of sight. The weaker cloud is found to be negligible for ^{6}Li. The isotopic ratio is 12.5.

Li isotopes measured for supernova remnant

Taylor et al. (2012)

-supernova remnant IC443
distance 1.5kpc
age 10,000-30,000 years

-Li absorption lines for background stars

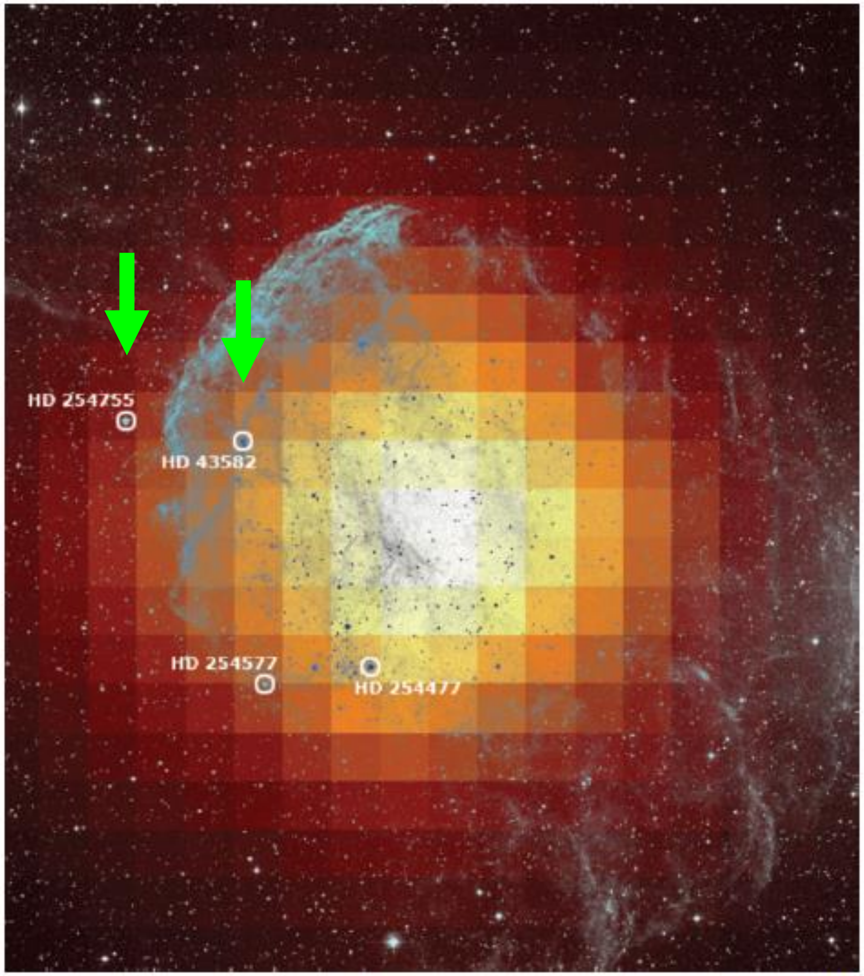

Figure 1. Composite image of IC 443. The optical image from the Digitized Sky Survey (POSS-II/red filter) is shown superimposed onto a gamma-ray intensity map in the 400 MeV to 3 GeV energy range obtained by the *Fermi* LAT (J. Hewitt 2011, private communication). The stars targeted for HET observations are labeled.

Li isotopes measured for supernova remnant

Outside of remnant **Inside of remnant**

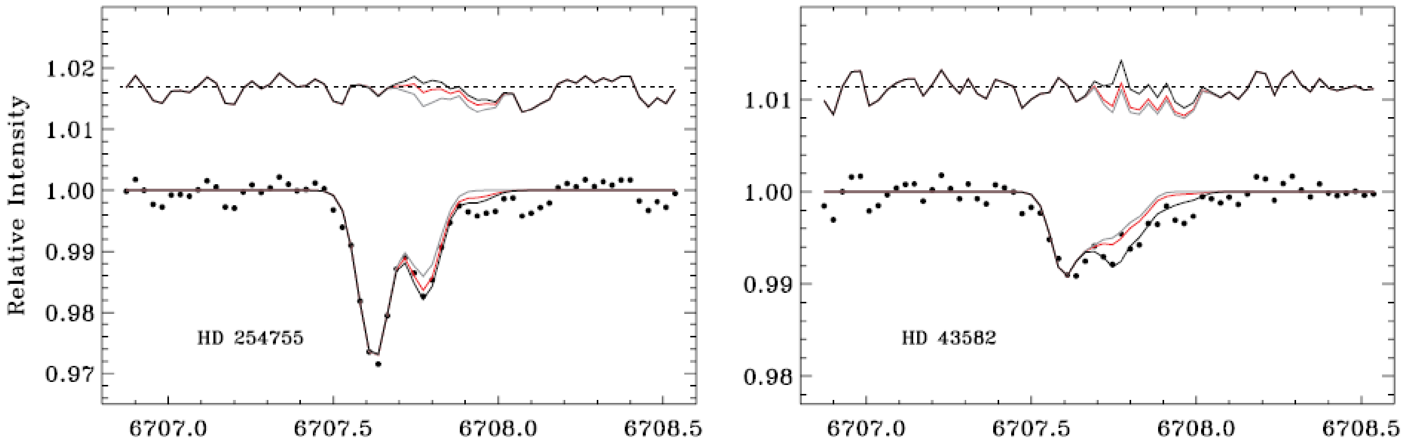

Wavelength (Å)

↓	↓
^{7}Li/^{6}Li=7.1±2.4	**^{7}Li/^{6}Li=3.1±1.4**
(‘normal’ ratio)	**Lower ratio**
	→production of ^{6}Li by
Taylor et al. (2012)	**cosmic-ray spallation?**